Antiferromagnetism in $CoCl_2 \cdot 2H_2O$. II. Chlorine Nuclear Magnetic Resonance and Paramagnetic Susceptibility*

ALBERT NARATH
Sandia Laboratory, Albuquerque, New Mexico
(Received 18 April 1965)

The chlorine NMR in $CoCl_2 \cdot 2H_2O$ has been studied in the paramagnetic and antiferromagnetic states. Zeeman-splitting studies in the paramagnetic state (76°K) yield $h^{-1}e^2qzzQ^{35}=9.866\pm0.001$ Mc/sec, $\eta=0.44\pm0.01$, and magnetic field shifts $(\Delta H/H_0)^{\alpha\alpha}=0.032\pm0.002$, $(\Delta H/H_0)^{\beta\beta}=0.112\pm0.002$, $(\Delta H/H_0)^{\gamma\gamma}=0.108\pm0.002$. The principal-axis orientations of the electric-field-gradient and field-shift tensors are $Z\|b$, $X\|(a^*-30°)$, and $\gamma\|b$, $\alpha\|(a^*+43°)$, respectively. In the antiferromagnetic state (4.0°K) zero-field resonances occur at (^{35}Cl) 6.576, 11.534, 16.415, (^{37}Cl) 5.702, 9.611, 13.460 (±0.002) Mc/sec. Using the paramagnetic-state asymmetry parameter, the observed frequencies yield $h^{-1}e^2qzzQ$: (^{35}Cl) 9.855, (^{37}Cl) 7.767 Mc/sec, and effective 0°K internal magnetic fields H_i: (^{35}Cl) 27.558, (^{37}Cl) 27.595 kOe. The internal field assignments correspond to a magnetic hyperfine anomaly for the two isotopes of $(1.3\pm0.4)\times10^{-3}$. The principal directions and principal values of the magnetic-susceptibility tensor have been determined in the paramagnetic state (20–120°K). The susceptibility is characterized by extreme rhombic anisotropy. The major axis (δ) coincides with b; the other two axes (ξ,ζ) nearly coincide with the Co–Cl bond directions. The measured principal values are analyzed on the basis of a two-parameter crystal field model which includes the effect of spin-orbit coupling. The chlorine magnetic hyperfine coupling constants in the paramagnetic state are evaluated by combining the field-shift measurements with spin expectation values obtained from the crystal field model. The results for ^{35}Cl are $A^{\xi\xi}=5.8(\pm0.3)\times10^{-4}$, $A^{\zeta\zeta}=6.85(\pm0.15)\times10^{-4}$, $A^{\delta\delta}=4.09(\pm0.08)\times10^{-4}$ cm^{-1}. A comparison of the paramagnetic and antiferromagnetic state results suggests that Cl-Cl interactions may contribute significantly to the transferred hyperfine field at the chlorine nucleus. The electric field gradient is compared with predictions of a point-charge model.

I. INTRODUCTION

THE work discussed in this report is part of a continuing study of the magnetic properties of dihydrated iron-group halides $MX_2 \cdot 2H_2O$ (M=Mn, Fe, Co; X=Cl, Br). This isomorphous series of compounds is distinguished by a relatively uncomplicated crystal structure in which the paramagnetic ions are situated in equivalent positions. Thus, bulk measurements can be related unambiguously to single-ion properties. The magnetic behavior of these compounds is of interest because the principal exchange paths involve metal-halogen linkages which are very similar to those responsible for magnetic-ordering phenomena in the corresponding anhydrous salts (e.g., $MnCl_2$, $FeCl_2$, $CoCl_2$). For this reason these compounds should provide useful information about the nature of indirect exchange interactions in transition-metal salts.

In a previous paper[1] (hereafter referred to as I) the magnetic structure of $CoCl_2 \cdot 2H_2O$ was determined from an analysis of single-crystal magnetic susceptibility and proton nuclear magnetic resonance (NMR) measurements. Approximate magnitudes of the principal exchange constants were inferred subsequently[2,3] on the basis of high-field magnetization experiments in the ordered state. The purpose of the present paper is to present the results of a detailed study of magnetic and electric hyperfine effects at the chlorine nuclei of $CoCl_2 \cdot 2H_2O$, in the paramagnetic as well as in the antiferromagnetic states.[4] During the course of this study the paramagnetic susceptibilities of $CoCl_2 \cdot 2H_2O$ were re-examined experimentally and analyzed in detail. As a result it has been possible to deduce the chlorine magnetic-hyperfine coupling constants in this compound based on a true-spin formalism.

The pertinent physical properties of $CoCl_2 \cdot 2H_2O$ are reviewed in Sec. II. The chlorine NMR results are presented in Sec. III. This section includes the necessary theoretical background, the experimental details of our resonance experiments, and the results of measurements in the paramagnetic and antiferromagnetic states. The magnetic susceptibility of $CoCl_2 \cdot 2H_2O$ in the paramagnetic state is discussed in Sec. IV. Experimental measurements of the temperature dependence of the principal elements of the susceptibility tensor are presented. The results are analyzed on the basis of a rhombic crystal-field perturbation of the lowest orbital triplet of Co^{2+} in the presence of spin-orbit coupling. The chlorine magnetic-hyperfine coupling constants are evaluated in Sec. V by combining the results of the two preceding sections. The experimentally determined elements of the electric-field-gradient tensor (EFG) are compared with predictions of a point-charge model in Sec. VI. Our results are summarized and discussed in Sec. VII.

II. REVIEW OF PHYSICAL PROPERTIES

The crystal structure of $CoCl_2 \cdot 2H_2O$ has monoclinic symmetry[5,6] (space-group $C2/m$) and is illustrated in

* This work was supported by the U. S. Atomic Energy Commission.

[1] A. Narath, Phys. Rev. **136**, A766 (1964).
[2] A. Narath, J. Phys. Soc. Japan **19**, 2244 (1964).
[3] A. Narath, Phys. Letters **13**, 12 (1964).
[4] A. Narath and D. W. Alderman, Bull. Am. Phys. Soc. **9**, 732 (1964).
[5] B. K. Vainshtein, Dokl. Akad. Nauk. SSSR **68**, 301 (1949).
[6] B. Morosin and E. J. Graeber, Acta Cryst. **16**, 1176 (1963).

Fig. 1. The room-temperature lattice parameters are given in Table I. The Co^{2+} ions are surrounded by a nearly perfect square-planar arrangement of Cl^- ions in (010) planes; the hydrate oxygens lie above and below these planes along [010]. There are two types of Co—Cl bonds which differ in length by about 1%. The important point-group symmetry elements at the cobalt positions are a two-fold axis parallel to the b axis, and a perpendicular mirror in the ac plane containing the chlorine ions. The unit cell contains two formula units which are related, however, by the lattice-centering operation. The structure consists of parallel, polymeric cobalt-chlorine ($-CoCl_2-$) chains which are linked together by weak hydrogen bonds. For this reason, crystals grown from saturated aqueous solution are in the form of slender, prismatic needles with a preferred growth axis parallel to the chain direction [001]. Single crystals usually have well-developed (110) type faces. Because of the weak binding between chains, the crystals cleave easily along [001]. Twinning on (100) planes occurs frequently. The dihydrate is not the stable hydrate at room temperature in the presence of water, and crystal growth requires temperatures near 70°C.

Measurements of the magnetic susceptibility[1,7] have shown that $CoCl_2 \cdot 2H_2O$ becomes magnetically ordered below 17.5°K. A specific-heat anomaly occurs at 17.20°K.[8] The ordered state is characterized by a collinear two-sublattice configuration in which ferromagnetic chains, parallel to the c axis, are arranged antiferromagnetically with respect to adjacent chains.[1] The magnetic anisotropy is very large and results in sublattice magnetization directions which coincide with the crystallographic b axis. The important exchange interactions are the ferromagnetic interactions (J_0) along the chains, the antiferromagnetic interactions (J_1) which couple adjacent chains, and the antiferromagnetic interactions (J_2) which couple *intra*sublattice spins along the a axis. The corresponding exchange energies have been deduced,[3] on the basis of Ising spins, $\sigma=\frac{1}{2}$, from high-field measurements in the antiferromagnetic state and susceptibility measurements in the paramagnetic state. The values obtained in this way are $J_0z_0/k_B=19$°K, $J_1z_1/k_B=-18$°K, and $J_2z_2/k_B=-2$°K, where k_B is Boltzmann's constant and z_0, z_1, z_2 are the number of neighbors which are coupled to a given spin by the corresponding exchange interaction.

TABLE I. Room-temperature lattice parameters and atomic coordinates of $CoCl_2 \cdot 2H_2O$.

$C2/m$: $a_0=7.256$ Å, $b_0=8.575$ Å, $c_0=3.554$ Å, $\beta=97°33'$			
Position	a	b	c
Co	0	0	0
Cl	0.2373	0	0.5582
O	0	0.2378	0
H	0.06	0.30	0.16

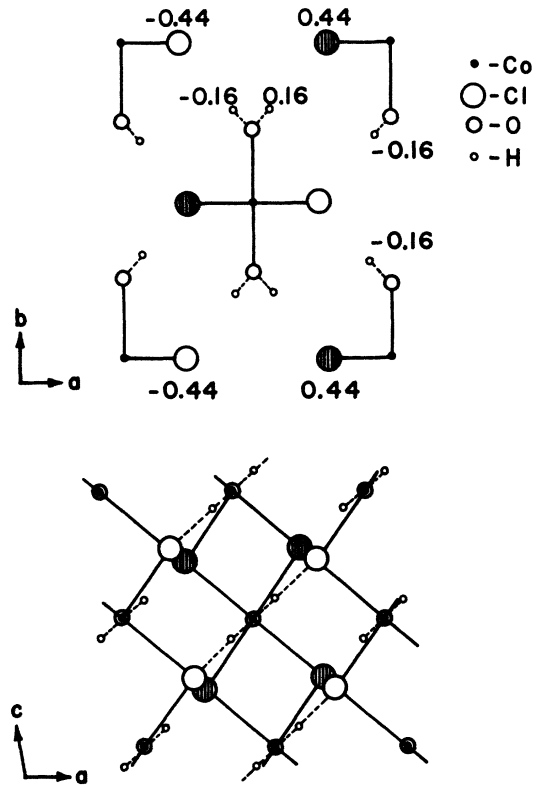

FIG. 1. Crystal structure of $CoCl_2 \cdot 2H_2O$. Top: projection along c axis on ab plane. Bottom: projection along b axis on ac plane.

III. CHLORINE NUCLEAR MAGNETIC RESONANCE

This section is concerned with the determination of the chlorine hyperfine interaction parameters in $CoCl_2 \cdot 2H_2O$. The isotopes of interest are ^{35}Cl and ^{37}Cl, whose respective natural abundances are 75.4 and 24.6%. Both isotopes have nuclear spins $I=\frac{3}{2}$. The corresponding magnetic dipole and electric quadrupole moments are $\mu^{35}=0.82089$ nm, $\mu^{37}=0.68329$ nm, and $Q^{35}=-0.07894$ b, $Q^{37}=-0.06213$ b, respectively.[9] The magnetic perturbations on the chlorine nucleus which must be considered in the analysis of our experiments arise from spin and orbital transferred hyperfine interactions (i.e., interactions with unpaired electrons in chlorine orbitals), Zeeman interactions with fields produced by surrounding magnetic moments and Zeeman interactions with externally applied fields. The electrostatic perturbations arise from interactions between the nuclear quadrupole moment and the nonuniform electric

[7] T. Haseda, H. Kobayashi, T. Watanabe and E. Kanda, in *Proceedings of the Eight International Conference on Low Temperature Physics* (Butterworths Scientific Publications Ltd., London, 1963); H. Kobayashi and T. Haseda, J. Phys. Soc. Japan 19, 765 (1964).

[8] T. Shinoda, H. Chihara, and S. Seki, J. Phys. Soc. Japan 19, 1637 (1964).

[9] V. Jaccarino and J. G. King, Phys. Rev. 83, 471 (1951).

field produced at the chlorine nucleus by the surrounding charge distribution.

A. Theoretical Background

The interactions discussed above lead to a Hamiltonian[10]

$$\mathcal{H}=\mathcal{H}_Q+\mathcal{H}_D, \tag{3.1}$$

where $\mathcal{H}_Q$ and $\mathcal{H}_D$ are the nuclear electric quadrupole and magnetic dipole Hamiltonians, respectively.

The quadrupole term of (3.1) is given by the scalar product of the nuclear quadrupole and electric field gradient tensors,

$$\mathcal{H}_Q=\{\mathbf{Q}\}\cdot\{\nabla\mathcal{E}\}, \tag{3.2}$$

where the curly brackets denote second-rank tensors. The Cartesian elements of $-\{\nabla\mathcal{E}\}$ are

$$V^{ij}=\partial^2V/\partial x^i\partial x^j, \quad (x^i, x^j=x, y, z) \tag{3.3}$$

where V is the electrostatic potential at the nucleus due to the surrounding charges and $\sum_i V^{ii}=0$. We denote the principal axes of $\{\nabla\mathcal{E}\}$ by X, Y, Z and let

$$\begin{aligned} eq&=V^{ZZ},\\ \eta&=(V^{XX}-V^{YY})/V^{ZZ}, \end{aligned} \tag{3.4}$$

where the usual convention $|V^{XX}|<V^{YY}|<|V^{ZZ}|$ has been followed. We thus obtain the standard form

$$\mathcal{H}_Q=\mathfrak{A}(3(I^Z)^2-I(I+1)+\tfrac{1}{2}\eta[(I^+)^2+(I^-)^2]), \tag{3.5}$$

where $\mathfrak{A}=e^2qQ/4I(2I-1)$ and Q is the scalar nuclear quadrupole moment.

The dipole term of (3.1) is given by

$$\mathcal{H}_D=-\gamma_N\hbar\mathbf{I}\cdot(\mathbf{H}_0+\mathbf{H}_i), \tag{3.6}$$

where γ_N is the nuclear gyromagnetic ratio, $2\pi\hbar$ is Planck's constant, $\mathbf{H}_0$ is the applied magnetic field, and $\mathbf{H}_i$ is the sum of all internally produced fields at the nucleus. In considering the origin of the internal field at the chlorine nucleus we make the usual assumption[11] at the outset that contributions from electrons in chlorine orbitals can be distinguished from those farther removed. Hence

$$\mathbf{H}_i=-(\gamma_N\hbar)^{-1}\{\mathbf{A}\}\cdot\mathbf{S}+2\mu_B\langle r^{-3}\rangle\mathbf{L}+\mathbf{H}_d, \tag{3.7}$$

where $\{\mathbf{A}\}$ is the magnetic-hyperfine coupling tensor, and μ_B is the Bohr magneton. The first two terms in (3.7) represent the spin- and orbital-hyperfine interactions with electrons localized at a given chlorine nucleus. The last term, $\mathbf{H}_d$, is the shape-dependent dipole field, which includes contributions from both spin- and orbital-magnetic moment distributions in the crystal, and is expected to be small compared with the hyperfine terms. It should be emphasized that $\langle r^{-3}\rangle$ and $\mathbf{L}$ in the orbital hyperfine term of (3.7) are to be evaluated with respect to the chlorine center. Thus it is the orbital angular momentum of the chlorine p states and not of the cobalt d states which determines the strength of the chlorine orbital hyperfine interaction. Because of the low symmetry at the chlorine site it is likely that the p orbital momentum is largely quenched. Therefore it will be assumed that the orbital hyperfine term can be neglected in the analysis of our chlorine NMR data. This assumption is necessary since the relative contributions of the spin- and orbital-hyperfine shifts of the nuclear resonance cannot be determined from our experiments.

We define a net field $\mathbf{H}$ acting on the nucleus

$$\mathbf{H}=\mathbf{H}_0+\mathbf{H}_i, \tag{3.8}$$

and examine the eigenvalues of (3.1). For $I=\frac{3}{2}$ and $H=0$ the eigenvalues can be obtained exactly.

$$E_m(0)=6\mathfrak{A}(|m|-1)(1+\tfrac{1}{3}\eta^2)^{\frac{1}{2}}, \tag{3.9}$$

where $m=\pm\frac{1}{2}, \pm\frac{3}{2}$ denotes the eigenvalues of I^Z. These doubly degenerate levels give rise to a single "pure quadrupole" resonance (NQR) frequency

$$\nu_0=\nu_Q(1+\tfrac{1}{3}\eta^2)^{\frac{1}{2}}, \tag{3.10}$$

where $\nu_Q=6\mathfrak{A}/h$. In the presence of a field which is sufficiently weak to satisfy $\gamma_NH/2\pi\ll\nu_Q$, the splitting of the degenerate levels is given to first order in H by

$$\begin{aligned} E_m(H)=E_m(0)\pm\tfrac{1}{2}\gamma_N\hbar H[&a_m^2\cos^2\theta\\ &+(b_m^2+c_m^2+2b_mc_m\cos2\phi)\sin^2\theta]^{\frac{1}{2}}. \end{aligned} \tag{3.11}$$

where θ, ϕ are the usual polar and azimuthal angles which specify the orientation of $\mathbf{H}$ in the X, Y, Z coordinate system, and

$$\begin{aligned} a_m&=-1-(4/\delta)(|m|-1),\\ b_m&=-1-(2/\delta)(|m|-1),\\ c_m&=(2\eta/\delta)(|m|-1),\\ \delta&=(1+\tfrac{1}{3}\eta^2)^{\frac{1}{2}}. \end{aligned} \tag{3.12}$$

There are four observable weak-field transitions corresponding to $\Delta m=\pm\frac{1}{2}\leftrightarrow\pm\frac{3}{2}$ (α transitions) and $\Delta m=\pm\frac{1}{2}\leftrightarrow\mp\frac{3}{2}$ (β transitions). For certain orientations of the field the two α transition frequencies coincide. Using (3.11), the locus (θ_0,ϕ_0) of zero α splitting is given by

$$\sin^2\theta_0(3-\eta\cos2\phi_0)-2=0. \tag{3.13}$$

When the Zeeman interaction is comparable in magnitude to the quadrupole interaction the perturbation treatment fails. In that case the eigenvalue problem, for a general field orientation, involves a Hermitian

[10] For a detailed review of this subject see T. P. Das and E. L. Hahn, *Nuclear Quadrupole Resonance Spectroscopy, Solid State Physics*, Suppl. 1 (Academic Press Inc., New York, 1958).

[11] M. Tinkham, Proc. Roy. Soc. (London) **A236**, 535 (1956); M. Tinkham, Proc. Roy. Soc. (London) **A236**, 549 (1956).

(complex) matrix, which for $I=\frac{3}{2}$ takes the form

$$\mathcal{H}=\begin{bmatrix} 3\mathcal{A}-\frac{3}{2}\gamma_N\hbar H^Z & (3^{\frac{1}{2}}/2)\gamma_N\hbar H^- & 3^{\frac{1}{2}}\mathcal{A}\eta & 0 \\ (3^{\frac{1}{2}}/2)\gamma_N\hbar H^+ & -3\mathcal{A}-\frac{1}{2}\gamma_N\hbar H^Z & \gamma_N\hbar H^- & 3^{\frac{1}{2}}\mathcal{A}\eta \\ 3^{\frac{1}{2}}\mathcal{A}\eta & \gamma_N\hbar H^+ & -3\mathcal{A}+\frac{1}{2}\gamma_N\hbar H^Z & (3^{\frac{1}{2}}/2)\gamma_N\hbar H^- \\ 0 & 3^{\frac{1}{2}}\mathcal{A}\eta & (3^{\frac{1}{2}}/2)\gamma_N\hbar H^+ & 3\mathcal{A}+\frac{3}{2}\gamma_N\hbar H^Z \end{bmatrix}, \tag{3.14}$$

where $H^{\pm}=H^X\pm iH^Y=He^{\pm i\phi}$. We consider the two special cases of (3.14) which occur in our experiments.

(*1*). $\mathbf{H}\|Z$. When the field is parallel to the Z axis of the EFG (i.e., $H^{\pm}=0$) the eigenvalues of (3.14) can be obtained exactly

$$\begin{aligned} E_{+\frac{3}{2}}(H^Z)&=-3\mathcal{A}[P(1+2R_{(-)})-R_{(-)}], \\ E_{+\frac{1}{2}}(H^Z)&=3\mathcal{A}[P(1-2R_{(+)})-R_{(+)}], \\ E_{-\frac{1}{2}}(H^Z)&=-3\mathcal{A}[P(1-2R_{(-)})+R_{(-)}], \\ E_{-\frac{3}{2}}(H^Z)&=3\mathcal{A}[P(1+2R_{(+)})+R_{(+)}], \end{aligned} \tag{3.15}$$

where

$$P=\gamma_N\hbar H/6\mathcal{A}, \tag{3.16}$$
$$R_{(\pm)}=[1+\tfrac{1}{3}\eta^2(2P\pm1)^{-2}]^{\frac{1}{2}}.$$

(*2*). $\mathbf{H}\perp Z$. When the field lies in the XY plane (i.e., $H^Z=0$) the complex-Hermitian form (3.14) can be transformed into a real-symmetric form which is convenient for rapid diagonalization by a digital computer. We carry out a unitary transformation $W^{-1}\mathcal{H}W=\mathcal{H}'$,

$$W=2^{-\frac{1}{2}}\times\begin{bmatrix} 1 & 0 & 0 & -i \\ 0 & 1 & -i & 0 \\ 0 & -i & 1 & 0 \\ -i & 0 & 0 & 1 \end{bmatrix}, \tag{3.17}$$

and obtain

$$\mathcal{H}'=3\mathcal{A}\times\begin{bmatrix} 1 & 3^{\frac{1}{2}}P\cos\phi & 3^{-\frac{1}{2}}\eta-3^{\frac{1}{2}}P\sin\phi & 0 \\ 3^{\frac{1}{2}}P\cos\phi & -1-2P\sin\phi & 2P\cos\phi & 3^{-\frac{1}{2}}\eta+3^{\frac{1}{2}}P\sin\phi \\ 3^{-\frac{1}{2}}\eta-3^{\frac{1}{2}}P\sin\phi & 2P\cos\phi & -1+2P\sin\phi & 3^{\frac{1}{2}}P\cos\phi \\ 0 & 3^{-\frac{1}{2}}\eta+3^{\frac{1}{2}}P\sin\phi & 3^{\frac{1}{2}}P\cos\phi & 1 \end{bmatrix}. \tag{3.18}$$

B. Experimental Details

The methods for growing single crystals of $CoCl_2 \cdot 2H_2O$ were identical to those discussed in I. Crystals were oriented by x-ray diffraction techniques within a maximum uncertainty of approximately $\pm0.5°$. The frequent occurrence of twinning on (100) planes was utilized in measurements requiring greater orientational accuracy. Since the resonance patterns in twinned crystals must be symmetric about a^* and c, these axes can be located very accurately.

In the paramagnetic state the chlorine resonances were observed initially with a super-regenerative detector.[12] Subsequent frequency measurements in the temperature range 55–300°K utilized a simple marginal oscillator[13] (Fig. 2), which was capable of operating at rf voltage levels of 1–10 V rms across the sample coil. In the antiferromagnetic state (4.0°K) the chlorine resonances saturate easily and hence the low-level marginal detector described in I was used. All of our resonance experiments utilized 200 cps sinusoidal field modulation and 400 cps synchronous detection.

Two types of external-field experiments were carried out. The first type consisted of measurements in a weak external field produced by a large volume, rotating, water-cooled Helmholtz coil. A field strength of 200 Oe was chosen for these experiments. This field was sufficiently weak to produce only a small perturbation on the quadrupole levels; on the other hand, it was sufficiently strong that the field orientation was not disturbed significantly by the earth's magnetic field. The second type of experiment required higher fields which were obtained in a Varian 12-in. rotating electromagnet.

Variable temperatures in the range 55–90°K were attained in pumped baths of liquid nitrogen and oxygen. Temperatures in this range were measured with copper-Constantan thermocouples. Experiments near the Néel temperature were performed with the sample immersed in a liquid-hydrogen bath; experi-

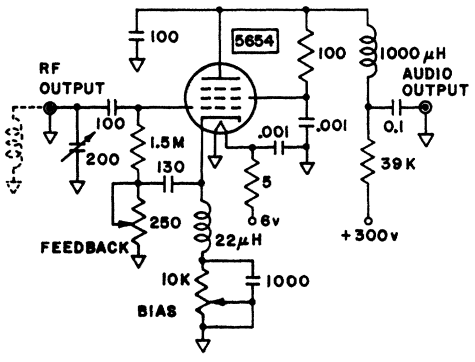

FIG. 2. Schematic of high-level marginal oscillator,

[12] A. Narath, W. J. O'Sullivan, W. A. Robinson, and W. W. Simmons, Rev. Sci. Instr. 35, 476 (1964).

[13] This circuit is derived from the rf oscillator section of a signal-feedback design given by T. Wang, Ref. 15.

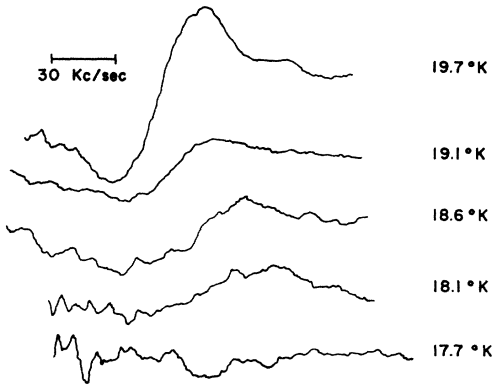

FIG. 3. Tracings of zero-field ^{35}Cl resonance patterns in $CoCl_2 \cdot 2H_2O$ near the Néel temperature. Signals were detected with a super-regenerative detector at a quench rate of 20 kc/sec, using sinusoidal magnetic field modulation at 200 cps and synchronous detection at 400 cps. The center frequency is approximately 5.07 Mc/sec.

ments in the antiferromagnetic state utilized a liquid-helium bath. In these experiments temperature measurements were based on the appropriate vapor pressure scale.

C. Paramagnetic State Experiments

In the following we describe experiments which were designed to give a quantitative measure of the elements of the electric and magnetic hyperfine interaction tensors. The determination of the principal-axis orientations of these tensors is simplified somewhat by crystal symmetry. The chlorine positions in $CoCl_2 \cdot 2H_2O$ have C_{1h} symmetry. Thus one of the principal axes of any chlorine-site tensor property coincides with the crystallographic b axis, and the two other principal axes lie in the ac plane. Furthermore, crystal symmetry requires that the principal-axis orientations are the same at every chlorine site.

A search for the zero-field chlorine resonances revealed a single resonance for each isotope.[14] The 294°K ^{35}Cl absorption occurs at $\nu_0^{35}=5.227\pm0.005$ Mc/sec. At 76°K the frequencies are $\nu_0^{35}=5.0895\pm0.0005$ Mc/sec and $\nu_0^{37}=4.011\pm0.001$ Mc/sec. The frequency ratio for the two isotopes is $\nu_0^{35}/\nu_0^{37}=1.2689\pm0.0003$ which is in good agreement with the accepted value[15] of 1.2688. In the range 55–300°K the observed linewidth (i.e., full width between first-derivative maxima) is $\sim$7 kc/sec independent of temperature. In the liquid-hydrogen range above T_N, however, the resonance was not observable with a marginal detector. The signals obtained with a superregenerative detector in this range are shown in Fig. 3. The source of the apparent line broadening to about 50 kc/sec is not understood.

The results of weak-field rotation studies about the c and b axes are shown in Fig. 4 and Fig. 5, respectively. A crossing of the α transitions is observed in the c rotation but not in the b rotation. An inspection of (3.13) shows that for $\eta<1$ an α overlap occurs for rotations through Z but not for rotations in the XY plane. Hence, the Z axis of the chlorine EFG tensor in $CoCl_2 \cdot 2H_2O$ coincides with the crystallographic b axis.

The measurements outlined in the preceding paragraph leave only two quadrupole parameters undetermined. These are η and the orientation λ_X of the X principal axis in the ac plane. In an attempt to determine these parameters, measurements of the α-crossing angles were performed at 76°K for several different field rotations through the b axis. The appropriate values of θ_0 in (3.13) were measured with an accuracy of $\pm0.10°$ by careful interpolation of measured frequencies near the α-crossing points. The oriented crystal was mounted on a goniometer which was immersed in liquid N_2 and positioned in the center of the Helmholtz coil. The angle λ_0 between a^* and the projection of H_0 on the ac plane could be set accurately by means of the goniometer without removing the crystal from the apparatus. For each rotation the measured values of λ_0 and θ_0 were substituted into (3.13) using the relation $\phi_0=\lambda_0-\lambda_X$, and the resulting values of η were plotted as a function of λ_X. The results are shown in Fig. 6. It is apparent that despite the accurate measurements of λ_0 and θ_0, only a very approximate solution for η and λ_X is obtained. The explanation for this apparent discrepancy is found in field-induced magnetic hyperfine effects. Although the determination of η from (3.13) does not depend on the magnitude of $\mathbf{H}$, it depends very sensitively on a knowledge of the orientation (ϕ_0,θ_0) of the net field $\mathbf{H}$ at the chlorine nucleus. Thus, if $\mathbf{H}_i$ (3.7) is anisotropic, the orientation of $\mathbf{H}$ will in general not coincide with that of the applied field $\mathbf{H}_0$.

At this point it is necessary to examine the form of $\mathbf{H}_i$ in the paramagnetic state. We have

$$\mathbf{H}_i-\mathbf{H}_d=-(\gamma_N\hbar)^{-1}\{\mathbf{A}\}\cdot\langle\mathbf{S}\rangle, \qquad (3.19)$$

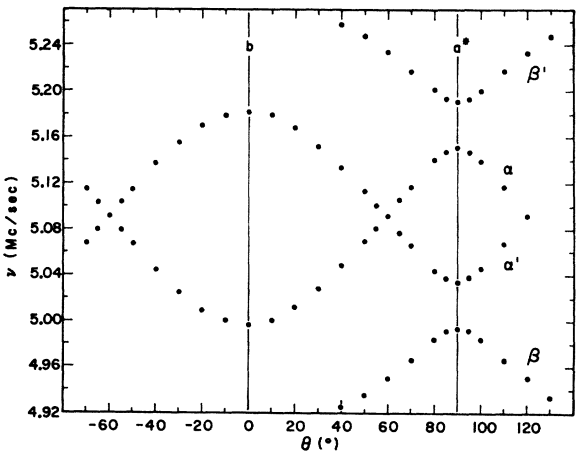

FIG. 4. Resonance diagram of ^{35}Cl in $CoCl_2 \cdot 2H_2O$ at 76°K for rotation of a 200 Oe magnetic field about the c axis.

[14] A. Narath, B. Morosin, and A. T. Fromhold, Jr., Bull. Am. Phys. Soc. 8, 359 (1963).
[15] T. Wang, Phys. Rev. 99, 566 (1955).

where $\langle \mathbf{S} \rangle$ is the average field-induced, temperature-dependent expectation value of $\mathbf{S}$, whose direction is not necessarily parallel to $\mathbf{H}_0$. We define a tensor $\{\mathbf{T}\}$ whose elements are given by

$$T^{ij} = \langle S^i \rangle / H_S{}^j, \tag{3.20}$$

where $\mathbf{H}_S$ is the effective field acting on $\mathbf{S}$. We then obtain

$$\mathbf{H}_i - \mathbf{H}_d = -(\gamma_N \hbar)^{-1} \{\mathbf{A}\} \cdot \{\mathbf{T}\} \cdot \mathbf{H}_S. \tag{3.21}$$

The validity of (3.21) depends on $\mathbf{H}_0$ being sufficiently small that saturation effects are unimportant. In order to make the problem of fitting (3.21) to experiment tractable it is convenient to assume that $\{\mathbf{A}\} \cdot \{\mathbf{T}\}$ has a symmetric tensor form. This assumption is clearly not always justified since the product of two real-symmetric matrices is not, in general, real-symmetric itself. In order for the matrix product to be real-symmetric the principal-axis directions of $\{\mathbf{A}\}$ and $\{\mathbf{T}\}$ must coincide, or one of the tensors must be isotropic in any principal plane of the other tensor in which the axes do not coincide. From the symmetry of $CoCl_2 \cdot 2H_2O$ it follows that the b axis is a principal axis common to both tensors. The relative orientations in the ac plane, however, are not specified by symmetry. We have, nevertheless, tried to fit a real-symmetric form for $\{\mathbf{A}\} \cdot \{\mathbf{T}\}$ to our experimental results and have found good agreement. The reasons for this agreement are discussed in Sec. V. In the meantime we take

$$\mathbf{H} = \mathbf{H}_0 + \{\Delta \mathbf{H}/\mathbf{H}_0\} \cdot \mathbf{H}_0, \tag{3.22}$$

where

$$\{\Delta \mathbf{H}/\mathbf{H}_0\} \cdot \mathbf{H}_0 = -(\gamma_N \hbar)^{-1} \{\mathbf{A}\} \cdot \{\mathbf{T}\} \cdot \mathbf{H}_S + \mathbf{H}_d. \tag{3.23}$$

Thus $\{\Delta \mathbf{H}/\mathbf{H}_0\}$ is the usual field-shift tensor which represents all of the modifications of the external field as seen by the chlorine nuclear moments.

At this point the solution of the problem of determining the elements of $\{\nabla \mathcal{E}\}$ and $\{\Delta \mathbf{H}/\mathbf{H}_0\}$ still requires the determination of two EFG parameters and four field-shift parameters. These are η, λ_X and $(\Delta H/H_0)^{\alpha\alpha}$, $(\Delta H/H_0)^{\beta\beta}$, $(\Delta H/H_0)^{\gamma\gamma}$, λ_α, respectively. The principal axes of $\{\Delta \mathbf{H}/\mathbf{H}_0\}$ are denoted by α, β, γ, with $\gamma \| Z$.

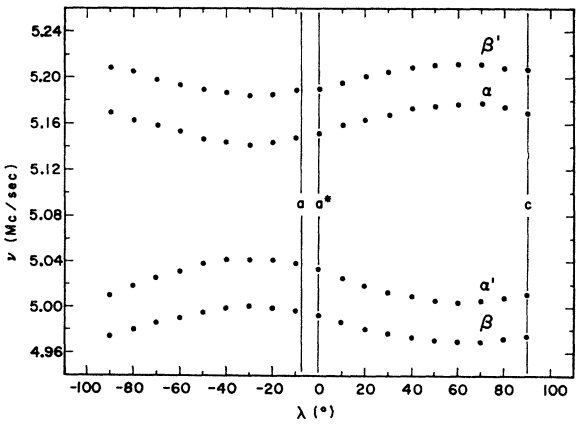

FIG. 5. Resonance diagram of ^{35}Cl in $CoCl_2 \cdot 2H_2O$ at 76°K for rotation of a 200 Oe magnetic field about the b axis.

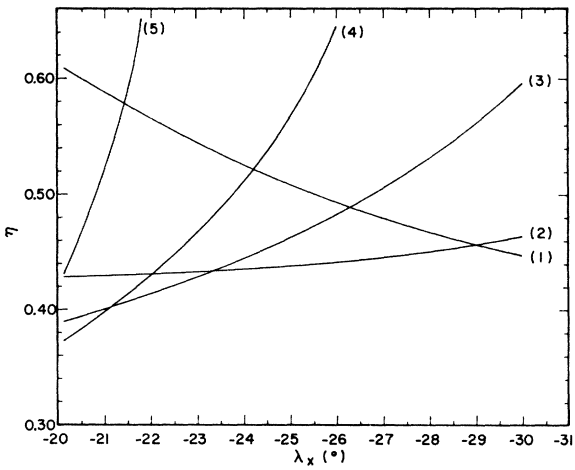

FIG. 6. Plot of 76°K α-crossing data for ^{35}Cl in $CoCl_2 \cdot 2H_2O$ according to Eq. (3.13). The numbered curves correspond to the experimental data listed in Table III.

The following iterative procedure for determining the hyperfine parameters was found to converge rapidly. Using approximate values of η and λ_X, best-fit values of the field-shift parameters were obtained from studies of one of the α transitions in fields of several kOe applied parallel and perpendicular to b. These field-shift parameters were then used in the following way to calculate corrected α-crossing angles (λ_0', θ_0') from the observed values (λ_0, θ_0). The field-shift tensor $\{\Delta \mathbf{H}/\mathbf{H}_0\}$ was transformed into the crystal-axis system ($x = a^*$, $y = c$, $z = b$) by rotating the α, β axes through an angle $-\lambda_\alpha$ in the xy plane. The components of $\mathbf{H}_0$ in the x, y, z system were calculated from λ_0 and θ_0. The components of $\mathbf{H}$ in this coordinate system were then obtained from (3.22) using the transformed field-shift tensor. The resulting directions of $\mathbf{H}$ are given by

$$\begin{aligned} \lambda_0' &= \tan^{-1}(H^y/H^x), \\ \theta_0' &= \tan^{-1}(H^y/H^z \sin\lambda_0'). \end{aligned} \tag{3.24}$$

Substitution of (3.24) into (3.13), using $\phi_0' = \lambda_0' - \lambda_X'$, gave a new solution for η and λ_X, which was subsequently utilized in a new fit of the high-field data. This process was repeated until a self-consistent set of parameters was obtained from the low- and high-field resonance data. During each cycle the comparison of the high-field α-resonance data with theory was based on computer solutions of (3.15) for $\mathbf{H}_0 \| b$ and (3.18) for $\mathbf{H}_0 \perp b$, using (3.22) in each case to compute both the magnitude as well as direction of the effective field $\mathbf{H}$.

The final results of the fitting procedure outlined above are listed in Table II. The agreement between experiment and theory which is obtained with these

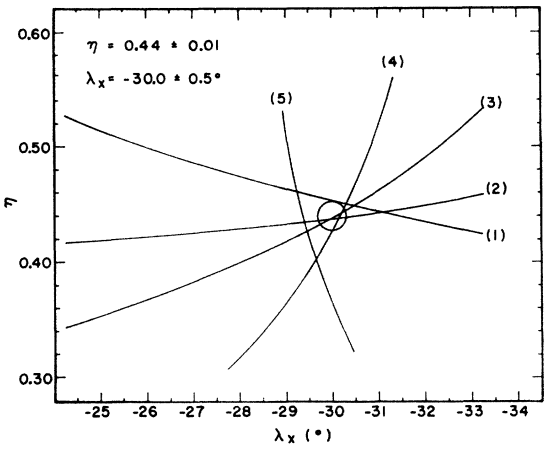

FIG. 7. Plot of 76°K α-crossing data for ^{35}Cl in $CoCl_2 \cdot 2H_2O$, corrected for shifts in the field direction resulting from field-induced hyperfine effects. The numbered curves refer to the adjusted data listed in Table III. The circle is an approximate representation of the estimated error limits for η and λ_X.

hyperfine parameters is illustrated in Fig. 7 for the α-crossing data, and in Fig. 8 for the high-field α-resonance data. The improvement in the self-consistency of the solution for η and λ_X (based on the corrected α-crossing angles listed in Table III) as revealed by a comparison of Fig. 6 and Fig. 7 is particularly gratifying. Furthermore, the rms deviation between calculated and observed fields for resonance in Fig. 8 using the parameters of Table II is 4 Oe. This deviation corresponds to approximately $\frac{1}{3}$ of the measured linewidth in these experiments. We conclude, therefore, that the magnetic hyperfine effects can be represented accurately by a symmetric field-shift tensor. The *ac*-plane orientations of the principal axes of $\{\Delta\mathbf{H}/\mathbf{H}_0\}$ and $\{\mathbf{\Delta}\mathcal{S}\}$ are related in Fig. 9 to the crystallographic environment of the chlorine ions.[16]

The temperature dependence of $\{\Delta\mathbf{H}/\mathbf{H}_0\}$ was studied in the range 55–90°K. Measurements on one of the α transitions were carried out in fields of about 4 kOe applied parallel to the principal axis directions (α,β,γ). The analysis was simplified by the fact that the zero-field resonance frequency was found to be temperature-independent in this range. Thus it was possible to assume that ν_Q and η remained constant. The results

TABLE II. Summary of chlorine magnetic-field-shift and quadrupole constants in $CoCl_2 \cdot 2H_2O$ at 76°K.

$(\Delta H/H_0)^{\alpha\alpha}=0.032\pm0.002$
$(\Delta H/H_0)^{\beta\beta}=0.112\pm0.002$
$(\Delta H/H_0)^{\gamma\gamma}=0.108\pm0.002$
$\lambda_\alpha=43\pm1°$ $(\gamma\|b)$

$e^2qQ^{35}/h=9.866\pm0.001$ Mc/sec
$\eta=0.44\pm0.01$
$\lambda_X=-30.0\pm0.5°$ $(Z\|b)$

[16] The 2.45 and 2.48 Å Co–Cl bond distances in Fig. 1(a) of Ref. 1 should be interchanged.

of the temperature dependence studies are shown in Fig. 10. It is noteworthy that $(\Delta H/H_0)^{\alpha\alpha}$ remains nearly constant while the two other principal elements exhibit a large variation with temperature.

D. Antiferromagnetic State Experiments

The antiferromagnetic state of $CoCl_2 \cdot 2H_2O$ is characterized by a two-sublattice magnetic structure as shown in I. The directions of sublattice magnetization coincide with the *b* axis. Since this is also a principal axis direction of the chlorine field-shift tensor, one expects to find a net magnetic hyperfine field oriented parallel to *b* in zero external field. The largest contribution to the transferred hyperfine field should arise from interactions between the Cl^- valence electrons with *d* electrons of the two nearest Co^{2+} ions. These ions have parallel spin orientations in the ordered state. Thus, the chlorine hyperfine field is related to the sum of the two individual cobalt contributions, as is also the case for the paramagnetic state. A rough estimate of the 0°K internal field based on a knowledge of the *b*-axis magnetic susceptibility indicated that the observable transitions should correspond to $\Delta m=\pm1$ at sufficiently low temperatures. From (3.15) we

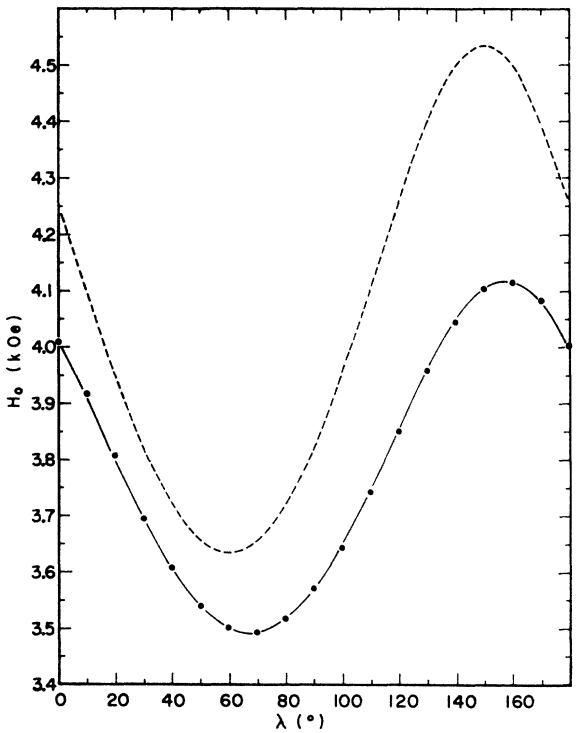

FIG. 8. Plot of ^{35}Cl α-resonance data at a constant frequency of 7.121 Mc/sec as a function of external field direction in the *ac* plane at 76°K. The experimental fields for resonance are plotted as points. The dashed curve represents the calculated resonance behavior on the basis of the quadrupole parameters given in Table II in the absence of magnetic hyperfine shifts; the solid curve represents the same calculation corrected for magnetic hyperfine effects according to the constants given in Table II.

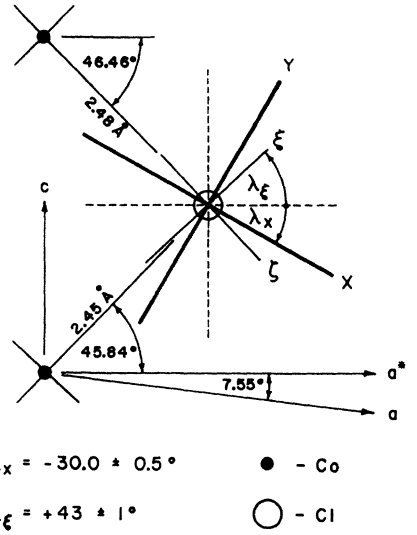

FIG. 9. Orientation of the principal axes of the chlorine EFG and magnetic-field-shift tensors in the *ac* plane.

obtain

$$\begin{aligned}
&\nu(+\tfrac{3}{2}\leftrightarrow+\tfrac{1}{2})\\
&\quad=\nu_Q[P(1-R_{(+)}+R_{(-)})-\tfrac{1}{2}(R_{(+)}-R_{(-)})],\\
&\nu(+\tfrac{1}{2}\leftrightarrow-\tfrac{1}{2})\\
&\quad=\nu_Q[-P(1-R_{(+)}-R_{(-)})+\tfrac{1}{2}(R_{(+)}-R_{(-)})],\\
&\nu(-\tfrac{1}{2}\leftrightarrow-\tfrac{3}{2})\\
&\quad=\nu_Q[P(1+R_{(+)}-R_{(-)})+\tfrac{1}{2}(R_{(+)}+R_{(-)})].
\end{aligned}\tag{3.25}$$

In the nearly saturated antiferromagnetic state we anticipate that $P>1$ and hence $R_{(\pm)}\approx 1$. Thus, the spectrum should consist of a triplet centered near $\nu=P\nu_Q=(\gamma_N/2\pi)H$ with nearly equal spacing given by $\Delta\nu=\pm\nu_Q$. A search at 4.0°K revealed the three predicted transitions for each chlorine isotope. The linewidths were approximately 10 kc/sec. In analyzing the transition frequencies it was assumed that η remains constant below 76°K. Agreement between the exact expression (3.25) and experiment was then achieved by adjusting ν_Q and P until a best fit was obtained. The ratio of ν_Q for the two isotopes was taken to be $\nu_Q^{35}/\nu_Q^{37}=1.2688$. The appropriate values of P, however, were determined separately for each isotope. The results of this fitting procedure are shown in Table IV. The value $\nu_Q^{35}(4.0°K)=4.9273$ Mc/sec compares very favorably with the 76°K result $\nu_Q^{35}(76°K)=4.9331$ Mc/sec. This suggests that no significant distortion of the lattice occurs on cooling through the magnetic-ordering transition, in agreement with preliminary results of x-ray diffraction measurements by Morosin.[17] The internal fields obtained from experiment are

$$\begin{aligned}
H_i^{35}&=27.558\pm0.005\text{ kOe},\\
H_i^{37}&=27.595\pm0.005\text{ kOe}.
\end{aligned}\tag{3.26}$$

TABLE III. Results of measurements of magnetic field orientations for which a zero-splitting of the chlorine α transitions is observed in $CoCl_2 \cdot 2H_2O$ at 76°K. The unprimed polar (θ_0) and azimuthal (λ_0) angles (measured relative to the b and a^* axes, respectively) give the external field ($\mathbf{H}_0$) orientations, while the primed angles give the orientations of the net field ($\mathbf{H}$) calculated on the basis of the field-shift parameters given in Table II. The tabulated angles are given in degrees and have estimated absolute uncertainties of ±0.10° for θ_0 and ±0.20° for λ_0.

Experiment	λ_0	θ_0	λ_0'	θ_0'
1	−45.75	60.90	−45.84	60.99
2	−18.67	61.85	−20.42	61.56
3	0.00	59.35	−2.14	58.46
4	11.33	57.20	9.39	55.90
5	20.00	55.75	18.42	54.16

TABLE IV. Comparison of calculated and observed chlorine nuclear resonance frequencies in antiferromagnetic $CoCl_2 \cdot 2H_2O$ at 4.0°K, in zero-external magnetic field.

Hyperfine parameters	ν (Mc/sec) Calculated	Observed
^{35}Cl: $\nu_Q=$ 4.9273 Mc/sec	16.416	16.415
$\eta=$ 0.44	11.532	11.534
$H_i=$27.558 kOe	6.577	6.576
^{37}Cl: $\nu_Q=$ 3.8834 Mc/sec	13.460	13.460
$\eta=$ 0.44	9.608	9.611
$H_i=$27.595 kOe	5.704	5.702

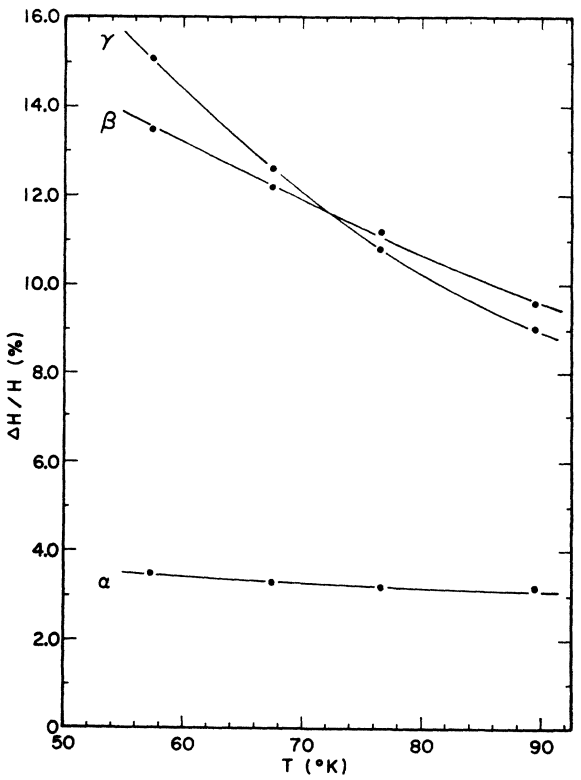

FIG. 10. Plot of the observed temperature dependence of the principal components of the chlorine magnetic-field-shift tensor in paramagnetic $CoCl_2 \cdot 2H_2O$. The solid lines are smooth fits to the data.

[17] B. Morosin (private communication).

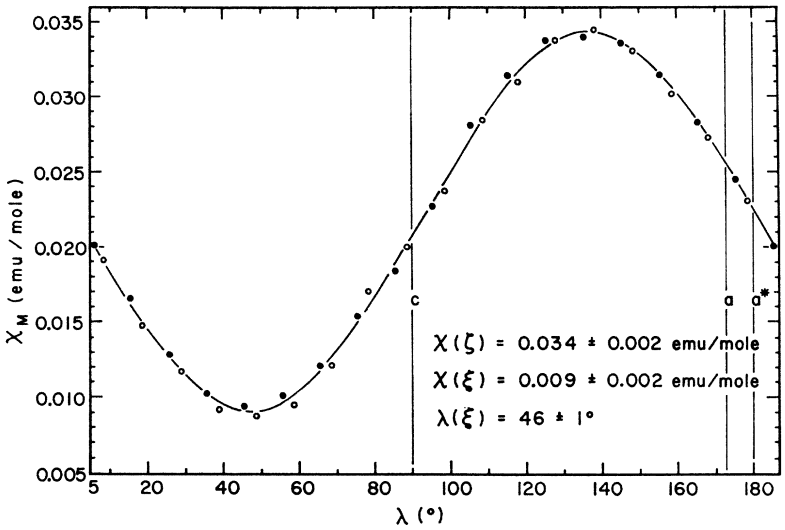

FIG. 11. Plot of the *ac*-plane magnetic susceptibility of $CoCl_2 \cdot 2H_2O$ at 76°K. The solid line is a smooth curve drawn through the data points.

The difference between these values lies well outside our experimental error and corresponds to a hyperfine anomaly of $(1.3\pm0.4)\times10^{-3}$. The internal fields (3.26) represent accurate 0°K estimates since no changes in the resonance frequencies were detected on cooling below 4.0°K.

The observation of only a single hyperfine field for a given isotope provides additional support for the two-sublattice magnetic structure given in I. The proposed magnetic space group retains the equivalence of all chlorine sites and is thus consistent with the results of our chlorine NMR studies. Finally, in order to verify the direction of $\mathbf{H}_i$ in the ordered state, the 4.0°K resonances were examined in external fields parallel to the b axis. The resonances were found to be split into two branches by the external field, one moving to higher frequencies and the other to lower frequencies. The observed splittings were in quantitative agreement with predictions of (3.25) based on the parameters of Table IV.

IV. MAGNETIC SUSCEPTIBILITY

In Sec. III the chlorine nuclear resonance data were treated in terms of a symmetric field-shift tensor. According to (3.23) the magnitudes of $H_d{}^i$ and T^{ij} must be known before the magnetic hyperfine tensor elements A^{ij} can be obtained from the measured $\{\Delta\mathbf{H}/\mathbf{H}_0\}$. The dipole field can be estimated readily if the crystal structure and magnetic susceptibility are known. In crystals in which the paramegnetic ions have orbitally nondegenerate ground states, the thermal expectation values of $\mathbf{S}$ can also be related in a simple way to the magnetic susceptibility. For Co^{2+} salts, however, the situation is more complicated. The orbital moment of Co^{2+} is not entirely quenched even for low site symmetries because of the spin-orbit interaction. It is necessary, therefore, to partition the susceptibilities according to orbital and spin contributions. In the following we discuss measurements of the single-crystal susceptibilities of $CoCl_2 \cdot 2H_2O$ and their interpretation based on a parametric model of the crystal field.

A. Experimental Measurements

The single-crystal susceptibilities of $CoCl_2 \cdot 2H_2O$ along the a^*, b, and c axes have been reported previously.[1,7] We denote the principal axes of the susceptibility tensor $\{\chi\}$ by ξ, ζ, δ. As before, one of the principal axes lies parallel to b (we take $\delta \| b$); the other two axes cannot be located by symmetry arguments. For this reason we have carried out a detailed examination of the *ac*-plane susceptibilities at 76°K. The apparatus was identical to that described previously.[18] The measured values were found to be highly sensitive to crystal imperfections. Most specimens whose cross sections normal to [001] exceeded a few millimeters were found to be twinned on (100) planes. This observation was verified by x-ray diffraction studies. The results of our measurements on two representative untwinned crystals are shown in Fig. 11. The anisotropy is seen to be quite pronounced. The minimum of the susceptibility occurs at $\lambda_\xi = 46\pm1°$, in close agreement with the minimum field-shift direction, $\lambda_\alpha = 43\pm1°$. This direction very nearly coincides with the short cobalt-chlorine bond direction (see Fig. 9). Twinned specimens usually exhibited susceptibilities which were nearly isotropic in (010), suggesting that twinning occurs during an early stage of crystal growth. This follows from the fact that the twin plane, (100), nearly bisects the observed principal-axis directions. The (010) susceptibility will therefore appear to be isotropic only if the two twin domains have equal volumes. Twinning of this type is observed in most large crystals of $CoCl_2 \cdot 2H_2O$ grown by the evaporation technique,

[18] A. Narath, Phys. Rev. 139, A1221 (1965).

which explains why the large (010) anisotropy escaped detection in earlier measurements.[1]

The temperature dependence of the principal susceptibilities in the paramagnetic state was studied in the range 20–120°K. The experimental techniques were the same as those described in I. The results are summarized in Fig. 12.

B. Theory

A meaningful treatment of the paramagnetic susceptibility of $CoCl_2 \cdot 2H_2O$ must take into account the rhombic symmetry of the crystal field as reflected in the measured anisotropies. In the following we examine the splitting of the free-ion levels of Co^{2+} under the combined influence of crystal-field and spin-orbit interactions.[19] The magnetic susceptibility is then calculated by a perturbation treatment of the effect of a magnetic field on the lowest levels.

The ^4F ($L=3$, $S=\frac{3}{2}$) free-ion ground state of Co^{2+} splits into two orbital triplets $^4T_1$, $^4T_2$ and an orbital singlet ^4A in a crystal field of cubic symmetry. One of the triplets ($^4T_1$) lies lowest in energy. The matrix elements of the orbital angular momentum $\mathbf{L}$ between states of $^4T_1$ are identical to those of $-\frac{3}{2}\mathbf{L}$ between the associated ^4P functions. The perturbation on these states due to noncubic distortions of the crystal field, and spin-orbit coupling can therefore be described by a zero-field Hamiltonian

$$\mathcal{H}_0 = -\tfrac{3}{2}k\lambda \mathbf{L}\cdot\mathbf{S} - \Delta[(L^\delta)^2 - \tfrac{2}{3}] + \Gamma[(L^\xi)^2 - (L^\zeta)^2], \quad (4.1)$$

where λ is the spin-orbit coupling constant, Δ is the axial distortion parameter, and Γ is the rhombic distortion parameter. The orbital reduction parameter k is of order unity and approximates the modification of the matrix elements of $\mathbf{L}$ due to covalent Co—Cl bonding and the cubic-field admixture of ^4P states into the ground state. We assume that these effects are isotropic. The perturbation (4.1) splits the 4×3-fold degeneracy of $^4T_1$ into six Kramers doublets. The corresponding zero-field energies are given by the roots of a sixth-order secular equation.

The perturbing Hamiltonian (4.1) ignores effects due to exchange interactions between cations. This neglect is justified by the observation (see I) that the magnetic susceptibilities can be fitted to a form

$$\chi^{rr} = [N(g^r\mu_B)^2\sigma(\sigma+1)/3k_B(T-\theta^r)] + N\alpha^r, \quad (4.2)$$

with $\theta^r \approx 0$, where χ^{rr} is the magnetic susceptibility of N ions in the rth principal direction, g^r is the g value based on an effective spin $\sigma=\frac{1}{2}$ ground state, k_B is Boltzmann's constant, T is the absolute temperature, θ^r is the Curie-Weiss constant, and α^r is a temperature-independent contribution arising primarily from high-frequency matrix elements of the paramagnetic moment. The absence of significant exchange effects in the paramagnetic state of $CoCl_2 \cdot 2H_2O$, despite its relatively high Néel temperature, is a consequence of ferromagnetic intrachain exchange energies which are essentially equal in magnitude to the antiferromagnetic interchain energies.

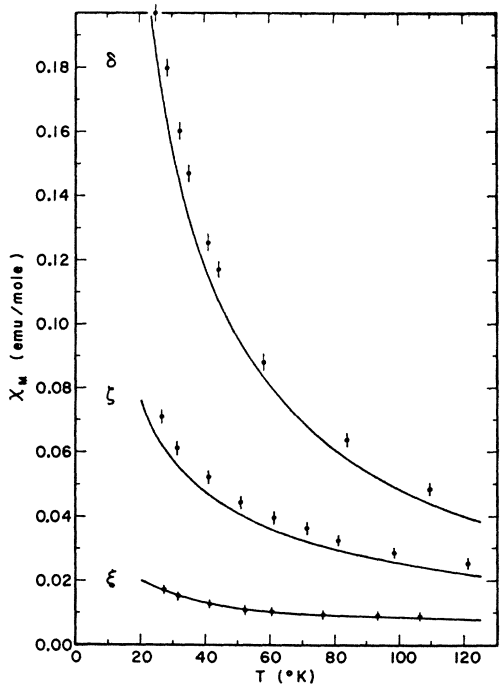

FIG. 12. Plot of the temperature dependence of the principal components of the $CoCl_2 \cdot 2H_2O$ magnetic-susceptibility tensor. The solid lines are best-fit theoretical curves based on calculations discussed in the text.

For a numerical evaluation of the eigenvalues of (4.1) it is convenient to define a new set of crystal-field parameters given by

$$\begin{aligned} \Delta &= \tfrac{1}{2}D(3+\kappa), \\ \Gamma &= \tfrac{1}{2}D(1-\kappa), \end{aligned} \quad (4.3)$$

where κ is an asymmetry parameter[20] which is restricted to the interval $-1 \leq \kappa \leq +1$. The Hamiltonian becomes

$$\mathcal{H}_0 = -\tfrac{3}{2}k\lambda \mathbf{L}\cdot\mathbf{S} + D[(L^\xi)^2 + \kappa(L^\zeta)^2 - (L^\delta)^2] - \tfrac{2}{3}D\kappa. \quad (4.4)$$

In the following we shall assume a $\mathbf{L}$, L^δ, $\mathbf{S}$, S^δ representation ($L=1$, $L^\delta=m_L$; $S=\frac{3}{2}$, $S^\delta=m_S$) with phases chosen in such a way that L^ξ, S^ξ are imaginary and L^ζ, S^ζ are real. The matrix elements of $\mathcal{H}_0$ obey the relations

$$\begin{aligned} \langle m_L, m_S|\mathcal{H}_0|m_L', m_S'\rangle &= \langle -m_L, -m_S|\mathcal{H}_0|-m_L', -m_S'\rangle \\ \langle m_L, m_S|\mathcal{H}_0|-m_L, -m_S\rangle &= 0. \end{aligned} \quad (4.5)$$

We shall denote the six states belonging to each of the

[19] The theory of the Co^{2+} energy levels in crystal fields of trigonal and tetragonal symmetries has been discussed in detail by A. Abragam and M. H. L. Pryce, Proc. Roy. Soc. (London) **A206**, 173 (1951).

[20] B. S. Ray, Z. Physik **78**, 74 (1932).

TABLE V. Calculated energies and effective g values of the six Kramers doublets derived from $^4T_1(^4F)$ in zero external field for $D/k\lambda=-7.0$, $\kappa=0.0$, $k=0.9$, and $\lambda=-176$ cm^{-1}. The orbital g values of the ground doublet include small corrections for the $^4T_2(^4F)$ admixture as discussed in the text.

$E_0/k\lambda$	$g_L{}^\xi$	$g_S{}^\xi$	$g_L{}^\zeta$	$g_S{}^\zeta$	$g_L{}^\delta$	$g_S{}^\delta$
−5.647	−1.69	5.68	−0.02	1.38	0.26	1.07
−5.156	0.63	−1.71	−0.26	2.48	0.47	−4.83
−0.826	−0.25	−0.65	0.11	−0.72	−1.64	5.80
0.585	1.13	4.37	0.17	−2.95	1.06	−1.99
5.093	0.14	−5.52	0.51	1.15	−0.16	−0.99
5.951	0.04	1.83	0.68	2.67	1.82	4.95

two degenerate sets by $|+\rangle$ and $|-\rangle$. We define a matrix $\mathbf{M}$

$$\mathbf{M}=\langle\pm|\mathcal{H}_0|\pm\rangle, \tag{4.6}$$

which yields the eigenvalues of $\mathcal{H}_0$ when brought into diagonal form by a unitary transformation $\mathbf{V}$

$$E_{0,i}=\langle i|\,\mathbf{V}^{-1}\mathbf{M}\mathbf{V}|i\rangle, \tag{4.7}$$

where the state index i takes the value 1 to 6.

We now introduce a magnetic field $\mathbf{H}$ which gives rise to an additional perturbation

$$\mathcal{H}_1=\mu_B\mathbf{H}\cdot(-\tfrac{3}{2}k\mathbf{L}+2\mathbf{S}). \tag{4.8}$$

We define a set of angular-momentum matrices

$$\begin{aligned}
&\mathbf{Z}_L{}^\xi=i\langle\pm|L^\xi|\mp\rangle, \quad \mathbf{Z}_S{}^\xi=i\langle\pm|S^\xi|\mp\rangle,\\
&\mathbf{Z}_L{}^\zeta=\langle\pm|L^\zeta|\mp\rangle, \quad \mathbf{Z}_S{}^\zeta=\langle\pm|S^\zeta|\mp\rangle,\\
&\mathbf{Z}_L{}^\delta=\langle\pm|L^\delta|\pm\rangle, \quad \mathbf{Z}_S{}^\delta=\langle\pm|S^\delta|\pm\rangle,
\end{aligned} \tag{4.9}$$

and apply the transformation which diagonalized $\mathcal{H}_0$. This gives

$$\mathfrak{Z}_L{}^r=\mathbf{V}^{-1}\mathbf{Z}_L{}^r\mathbf{V}, \quad \mathfrak{Z}_S{}^r=\mathbf{V}^{-1}\mathbf{Z}_S{}^r\mathbf{V}, \tag{4.10}$$

where r specifies one of the principal axes, $r=\xi,\zeta,\delta$. If we restrict $\mathbf{H}$ to one of these directions we obtain a splitting $\pm\mathfrak{P}^rH^r$ of the Kramers degeneracies, where

$$\mathfrak{P}^r=(K_L{}^r\mathfrak{Z}_L{}^r+K_S{}^r\mathfrak{Z}_S{}^r)/H^r, \tag{4.11}$$

with

$$\begin{aligned}
K_L{}^r&=-\tfrac{3}{2}k\mu_BH^r,\\
K_S{}^r&=2\mu_BH^r.
\end{aligned} \tag{4.12}$$

The effect of (4.11) on the six doublet states can be calculated by perturbation theory. The results, to second order in H, are

$$E_i{}^r=E_{0,i}\pm\langle i|\mathfrak{P}^r|i\rangle+\sum_{j\neq i}\frac{[\langle i|\mathfrak{P}^r|j\rangle]^2}{E_{0,i}-E_{0,j}}. \tag{4.13}$$

The spin- and orbital-magnetic interactions have been treated separately up to this point since the interpretation of our chlorine field-shift parameters requires a knowledge of the thermal expectation values of $\mathbf{S}$. The expectation values of $\mathbf{L}$ and $\mathbf{S}$ in the perturbed states of (4.13) can be calculated using the Hellmann-Feynman theorem.[21] We obtain

$$\begin{aligned}
L_i{}^r&=\partial E_i{}^r/\partial K_L{}^r,\\
S_i{}^r&=\partial E_i{}^r/\partial K_S{}^r,
\end{aligned} \tag{4.14}$$

and, therefore, using (4.11)

$$\begin{aligned}
L_i{}^r&=\langle i|\mathfrak{Z}_L{}^r|i\rangle\\
&\quad+2\sum_{j\neq i}\left\{\frac{K_S{}^r\langle i|\mathfrak{Z}_L{}^r|j\rangle\langle i|\mathfrak{Z}_S{}^r|j\rangle+K_L{}^r(\langle i|\mathfrak{Z}_L{}^r|j\rangle)^2}{E_{0,i}-E_{0,j}}\right\},\\
S_i{}^r&=\langle i|\mathfrak{Z}_S{}^r|i\rangle\\
&\quad+2\sum_{j\neq i}\left\{\frac{K_L{}^r\langle i|\mathfrak{Z}_L{}^r|j\rangle\langle i|\mathfrak{Z}_S{}^r|j\rangle+K_S{}^r(\langle i|\mathfrak{Z}_S{}^r|j\rangle)^2}{E_{0,i}-E_{0,j}}\right\}.
\end{aligned} \tag{4.15}$$

The thermal averages of (4.15) are calculated in the usual way. For example,

$$\langle S^r\rangle=\frac{\sum_i S_i{}^r\exp(-E_i{}^r/k_BT)}{\sum_i\exp(-E_i{}^r/k_BT)}. \tag{4.16}$$

This expression can be simplified if $\mu_BH\ll k_BT$. It follows that, to first order in H^r,

$$\begin{aligned}
\frac{\langle S^r\rangle}{\mu_BH^r}&=[\textstyle\sum_i\exp(-E_{0,i}/k_BT)]^{-1}\\
&\quad\times\sum_i\left\{\exp(-E_{0,i}/k_BT)\left[-\frac{\langle i|\mathfrak{Z}_S{}^r|i\rangle\langle i|\mathfrak{P}^r|i\rangle}{k_BT}\right.\right.\\
&\quad\left.\left.+2\sum_{j\neq i}\frac{\langle i|\mathfrak{Z}_S{}^r|j\rangle\langle i|\mathfrak{P}^r|j\rangle}{E_{0,i}-E_{0,j}}\right]\right\}.
\end{aligned} \tag{4.17}$$

In the same way we obtain

$$\begin{aligned}
\frac{\langle L^r\rangle}{\mu_BH^r}&=[\textstyle\sum_i\exp(-E_{0,i}/k_BT)]^{-1}\\
&\quad\times\sum_i\left\{\exp(-E_{0,i}/k_BT)\left[-\frac{\langle i|\mathfrak{Z}_L{}^r|i\rangle\langle i|\mathfrak{P}^r|i\rangle}{k_BT}\right.\right.\\
&\quad\left.\left.+2\sum_{j\neq i}\frac{\langle i|\mathfrak{Z}_L{}^r|j\rangle\langle i|\mathfrak{P}^r|j\rangle}{E_{0,i}-E_{0,j}}\right]\right\}.
\end{aligned} \tag{4.18}$$

The paramagnetic susceptibility is given by

$$\chi^{rr}=\mu_BN(\tfrac{3}{2}k\langle L^r\rangle-2\langle S^r\rangle)/H^r. \tag{4.19}$$

Combining (4.17) and (4.18) according to (4.19) yields the standard Langevin-Debye susceptibility[22] appropriate for the Hamiltonian used here.

Finally, we derive orbital and spin g values for the

[21] H. Hellmann, *Einführung in die Quantenchemie* (Franz Deuticke, Leipzig, 1937); R. P. Feynman, Phys. Rev. 56, 340 (1939).

[22] J. H. Van Vleck, *The Theory of Electric and Magnetic Susceptibilities* (Oxford University Press, New York, 1932).

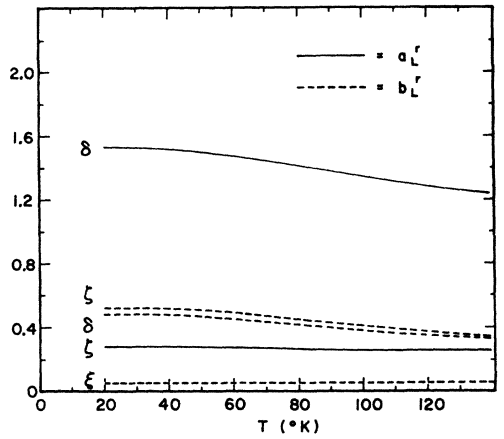

FIG. 13. Plot of the calculated thermal expectation values of the $CoCl_2 \cdot 2H_2O$ orbital angular momentum as a function of temperature. The solid curves represent the $a_L{}^r$ coefficients [in units of $°K-(10^6\ Oe)^{-1}$]; the dashed curves represent the $b_L{}^r$ coefficients [in units of $(10^6\ Oe)^{-1}$]. The coefficients are defined in Eq. (4.24). The magnitude of $a_L{}^\xi$ is too small to be plotted.

six effective-spin-$\frac{1}{2}$ Kramers doublets. These are

$$g_{L,i}{}^r = -3k\langle i|\mathfrak{Z}_L{}^r|i\rangle, \qquad g_{S,i}{}^r = 4\langle i|\mathfrak{Z}_S{}^r|i\rangle, \tag{4.20}$$

and lead to a total effective-g value for the r direction

$$g_i{}^r = g_{L,i}{}^r + g_{S,i}{}^r. \tag{4.21}$$

The expressions derived above were used to analyze the measured susceptibilities in the range 20–120°K. A program was written for the CDC-3600 digital computer to carry out the necessary calculations. For a given choice of D and κ the eigenvalues and eigenvectors of (4.4) were determined, and the orbital and spin angular momentum matrices transformed according to (4.10) to give the corresponding g values (4.20). The thermal expectation values of $\mathbf{L}$ and $\mathbf{S}$ were then computed for several temperatures according to (4.18) and (4.17), respectively. Finally, the magnetic susceptibility was calculated using (4.19). A fit of the theory to the experimental susceptibilities was attempted for $k=0.9$ and $\lambda=-176\ cm^{-1}$. In addition, a small correction was made for the admixture of $^4T_2$ into $^4T_1$ due to the spin-orbit and rhombic crystal-field terms in the Hamiltonian. This admixture enhances the matrix elements of $\mathfrak{Z}_L{}^r$ by a few percent while those of $\mathfrak{Z}_S{}^r$ are only affected in higher order. We have included this correction only in the diagonal matrix element of $\mathfrak{Z}_L{}^r$ for the lowest Kramers doublet. The magnitude of the correction was estimated from calculations by Abragam and Pryce[19] for the Co Tutton salts. We adjusted $\mathfrak{Z}_L{}^r$ by adding $(0.15/1.5k)$, $(0.10/1.5k)$, and 0 to $\mathfrak{Z}_L{}^\delta$, $\mathfrak{Z}_L{}^\zeta$, and $\mathfrak{Z}_L{}^\xi$, respectively.

The best agreement between theory and experiment is obtained for

$$D/k\lambda = -7.0\pm1.5, \qquad \kappa = 0.0\pm0.1, \tag{4.22}$$

as shown in Fig. 12. The calculated values of $\chi^{\zeta\zeta}$ and $\chi^{\delta\delta}$ are slightly too small. The general shape of the susceptibility-versus-temperature behavior, however, is reproduced very well. In view of the simplifications which are inherent in the model, such as the assumption of an isotropic orbital reduction factor, the agreement is quite satisfactory. The parameters in (4.22) correspond to

$$\Delta = 1.7(\pm0.4)\times10^3\ cm^{-1}, \qquad \Gamma = 0.55(\pm0.12)\times10^3\ cm^{-1}. \tag{4.23}$$

The calculated zero-field energies and g values for the above choice of crystal-field parameters are listed in Table V.

According to (4.17) and (4.18) the thermal expectation values of L^r and S^r may be written in the form

$$\langle L^r\rangle/H^r = a_L{}^r\left(\frac{100}{T}\right)+b_L{}^r, \qquad \langle S^r\rangle/H^r = a_S{}^r\left(\frac{100}{T}\right)+b_S{}^r, \tag{4.24}$$

where the coefficients are, in general, a function of temperature. The calculated values are shown in Fig. 13 and Fig. 14. The most significant feature of these plots is the marked increase of $|a_S{}^\xi|$ with increasing temperature. This behavior is a consequence of the large $g_S{}^\xi$ value of the first-excited doublet relative to that of the ground state (Table V). Accordingly, one predicts a very small temperature dependence for $\langle S^\xi\rangle$ in the

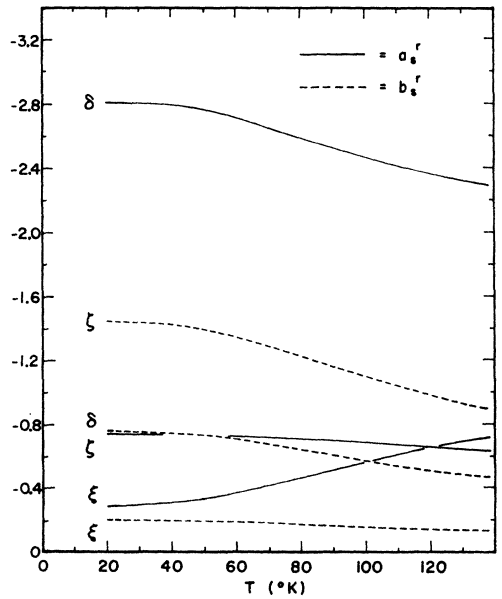

FIG. 14. Plot of the calculated thermal expectation values of the $CoCl_2 \cdot 2H_2O$ spin angular momentum as a function of temperature. The notation and units correspond to those used in Fig. 13.

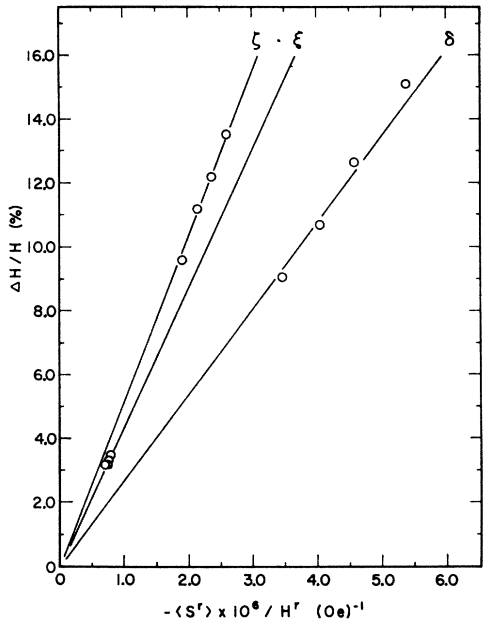

FIG. 15. Plot of measured chlorine field shifts in paramagnetic $CoCl_2 \cdot 2H_2O$ as a function of the calculated thermal-average spin expectation value. Temperature is the implicit variable.

region 55–90°K and thus a small temperature coefficient for $(\Delta H/H_0)^{\xi\xi}$, as shown in more detail in the following section.

V. CHLORINE MAGNETIC-HYPERFINE COUPLING CONSTANTS

It is now possible to calculate the magnitude of the chlorine hyperfine constants in $CoCl_2 \cdot 2H_2O$, based on the information presented in the two preceding sections. In the following, the principal elements of $\{\mathbf{A}\}$ will be calculated from the paramagnetic-state data. The results will then be compared with the antiferromagnetic-state observations.

A. Paramagnetic-State Analysis

In Sec. III(c) it was demonstrated that the chlorine NMR measurements are consistent with an internal magnetic field which is related to the external field through a symmetric second-rank field-shift tensor. It was also shown that this relationship is to be expected only if the principal axis directions of $\{\Delta\mathbf{H}/\mathbf{H}_0\}$ and $\{\mathbf{A}\}$ in the *ac* plane coincide, or if either tensor is isotropic in that plane. On the basis of independent measurements presented in this paper it appears that λ_α and λ_ξ are nearly equal. Although the difference of 3° lies outside the combined stated uncertainties of 2° we shall assume that the two directions are not distinguishable in our experiments, thus satisfying the above requirement. This assumption is supported by the observation that the susceptibility axes in the *ac* plane almost coincide with the Co—Cl bond directions.

Since the Co—Cl—Co angle is near 90° and since transferred hyperfine effects are dominated by bonding electrons it is not surprising that any anisotropic component of $\{\mathbf{A}\}$ would have its principal axes oriented along the Co—Cl bonds.

The calculation of $\{\mathbf{A}\}$ from $\{\Delta\mathbf{H}/\mathbf{H}_0\}$ using (3.23) requires a knowledge of $\mathbf{H}_d$, $\mathbf{H}_S$, and $\{\mathbf{T}\}$. The dipole field can be expressed with sufficient accuracy by a sum over point dipoles situated at the Co^{2+} lattice positions

$$\mathbf{H}_d = \{\mathfrak{D}\} \cdot \boldsymbol{\mu}, \tag{5.1}$$

where $\boldsymbol{\mu}$ is the magnetic moment per Co^{2+} ion. The Cartesian elements of $\{\mathfrak{D}\}$ are given by lattice sums of the form

$$^{ij}\mathfrak{D} = \sum (3x^i x^j - \delta_{ij} r^2)/r^5. \tag{5.2}$$

By direct summation of (5.2) over all Co^{2+} moments situated within a sphere of radius 200 Å centered at a given Cl^- position we find (using the lattice constants of Table I and coordinate axes which coincide with the principal-axis directions of $\{\chi\}$)

$$\{\mathfrak{D}\} = 10^{24} \times \begin{matrix} \\ \\ \\ \end{matrix} \begin{matrix} \xi & \zeta & \delta \\ \end{matrix} \begin{bmatrix} 0.05506 & 0.00838 & 0 \\ 0.00838 & 0.06185 & 0 \\ 0 & 0 & -0.11691 \end{bmatrix} \text{cm}^{-3}. \tag{5.3}$$

The Co^{2+} magnetic moment in the paramagnetic state can be obtained from the magnetic susceptibility. Thus, the components of $\mathbf{H}_d$ become

$$\begin{aligned} H_d{}^\xi &= 0.0914\chi^{\xi\xi}H_0{}^\xi + 0.0139\chi^{\zeta\zeta}H_0{}^\zeta, \\ H_d{}^\zeta &= 0.1027\chi^{\zeta\zeta}H_0{}^\zeta + 0.0139\chi^{\xi\xi}H_0{}^\xi, \\ H_d{}^\delta &= -0.1940\chi^{\delta\delta}H_0{}^\delta, \end{aligned} \tag{5.4}$$

where the susceptibilities are expressed in units of emu/mole. For typical values of χ^{rr} the transverse component of $\mathbf{H}_d$ in the *ac* plane can be neglected. The above calculation of $\mathbf{H}_d$ assumes a spherical sample shape. For nonspherical specimens there is an additional contribution whose magnitude is the difference between the Lorentz and demagnetizing fields. The crystals used in the present study had prismatic shapes. The shape effect for our samples is expected to be most severe for $\mathbf{H}_0 \| b$. However, we estimate that the effect on $(\Delta H/H_0)^{\delta\delta}$ is only of the order of 0.1% and can thus be neglected.

Since exchange effects are not very important in the paramagnetic state and since the field-induced dipole fields are small, it is possible to replace the field $\mathbf{H}_S$ in (3.23) by $\mathbf{H}_0$. The principal components of $\{\Delta\mathbf{H}/\mathbf{H}_0\}$ can therefore be written as

$$(\Delta H/H_0)^{rr} = -(\gamma_N \hbar)^{-1} A^{rr} (\langle S^r \rangle / H_0{}^r) + H_d{}^r / H_0{}^r. \tag{5.5}$$

The variation of $\{\chi\}$ with temperature is not very different from that of $\langle S^r \rangle$. Hence, the field-shift parameters should be a linear function of $\langle S^r \rangle / H_0{}^r$. This is demonstrated in Fig. 15, where use has been made of

the thermal expectation values of S^r calculated in Sec. IV. It is significant that the field-shift parameters are directly proportional to the calculated values of $\langle S^r \rangle$, since this behavior is a necessary condition for the validity of the crystal-field calculations. The weak temperature dependence of $(\Delta H/H_0)^{\xi\xi}$ is related to the very weak temperature dependence of $\langle S^r \rangle$ predicted by the theory. The slopes of Fig. 15 give the following field shifts per unit spin.

$$\begin{aligned} \Delta H^\xi/\langle S^\xi \rangle &= -44 \pm 3 \text{ kOe}, \\ \Delta H^\zeta/\langle S^\zeta \rangle &= -50.9 \pm 1.0 \text{ kOe}, \\ \Delta H^\delta/\langle S^\delta \rangle &= -26.5 \pm 0.6 \text{ kOe}. \end{aligned} \tag{5.6}$$

Using the measured susceptibilities, the field shifts in (5.6) can be adjusted for dipolar effects according to (5.4) and (5.5) to give the following hyperfine fields per unit spin:

$$\begin{aligned} H_{\rm hf}{}^\xi/\langle S^\xi \rangle &= -42 \pm 3 \text{ kOe}, \\ H_{\rm hf}{}^\zeta/\langle S^\zeta \rangle &= -49.3 \pm 1.0 \text{ kOe}, \\ H_{\rm hf}{}^\delta/\langle S^\delta \rangle &= -29.4 \pm 0.6 \text{ kOe}, \end{aligned} \tag{5.7}$$

where

$$H_{\rm hf}{}^r = -(\gamma_N \hbar)^{-1} A^{rr} \langle S^r \rangle. \tag{5.8}$$

Thus, the magnetic hyperfine constants for the two chlorine isotopes are

$$\begin{aligned} {}^{35}\text{Cl}: \quad & A^{\xi\xi} = 5.8(\pm 0.4) \times 10^{-4} \text{ cm}^{-1}, \\ & A^{\zeta\zeta} = 6.85(\pm 0.15) \times 10^{-4} \text{ cm}^{-1}, \\ & A^{\delta\delta} = 4.09(\pm 0.08) \times 10^{-4} \text{ cm}^{-1}, \\ {}^{37}\text{Cl}: \quad & A^{\xi\xi} = 4.8(\pm 0.3) \times 10^{-4} \text{ cm}^{-1}, \\ & A^{\zeta\zeta} = 5.71(\pm 0.10) \times 10^{-4} \text{ cm}^{-1}, \\ & A^{\delta\delta} = 3.40(\pm 0.05) \times 10^{-4} \text{ cm}^{-1}. \end{aligned} \tag{5.9}$$

The error limits given in (5.7) and (5.9) represent the estimated experimental uncertainties in the determination of $\{\Delta \mathbf{H}/\mathbf{H}_0\}$. Possible errors in the calculation of $\langle S^r \rangle$ are not included since their magnitude is difficult to estimate. We feel, however, that the quoted hyperfine constants have absolute accuracies of better than $\pm 10\%$. The most uncertain coupling constant is probably $A^{\xi\xi}$ since $\langle S^\xi \rangle$ includes appreciable contributions from the first excited doublet in the temperature range of our experiments. The magnitudes of the hyperfine constants are not necessarily the same, however, for different electronic states as assumed (by necessity) in the preceding analysis.

It is instructive to separate the hyperfine constants in the usual way[11] into isotropic (A_s) and anisotropic $(A_p{}^\xi, A_p{}^\zeta, A_p{}^\delta)$ contributions. The isotropic contribution arises from contact interactions with unpaired spins in chlorine s orbitals and is proportional to the net spin density at the nucleus. The anisotropic contributions arise from dipolar interactions with unpaired spins in chlorine p orbitals and are proportional to the expectation value of r^{-3} for these states. The three anisotropic contributions to A^{rr} have the form $A_p{}^r$ $(3\cos^2\theta - 1)$, where θ is the angle between $\mathbf{S}$ and $\mathbf{r}$. Since only three independent measurements are available, we can only determine A_s and pair-wise differences between the $A_p{}^r$.

$$A_s = \tfrac{1}{3} \textstyle\sum_r A^{rr} \tag{5.10}$$

$$A_p{}^r - A_p{}^{r'} = \tfrac{1}{3}(A^{rr} - A^{r'r'}). \tag{5.10}$$

For ^{35}Cl, we find

$$\begin{aligned} {}^{35}\text{Cl}: \quad & A_s = +5.58(\pm 0.20) \times 10^{-4} \text{ cm}^{-1}, \\ & A_p{}^\xi - A_p{}^\zeta = -0.3(\pm 0.2) \times 10^{-4} \text{ cm}^{-1}, \\ & A_p{}^\xi - A_p{}^\delta = +0.6(\pm 0.2) \times 10^{-4} \text{ cm}^{-1}, \\ & A_p{}^\zeta - A_p{}^\delta = +0.9(\pm 0.1) \times 10^{-4} \text{ cm}^{-1}. \end{aligned} \tag{5.11}$$

It is interesting to note that the magnetic hyperfine interaction is dominated by the contact term, A_s. Furthermore, within our experimental uncertainty, the degree of spin unpairing in the chlorine p^ξ and p^ζ orbitals is identical. The lack of anisotropy in the ac-plane hyperfine interaction is in striking contrast to the large anisotropy of the Co^{2+} magnetic moment. The large ac anisotropy of $\{\chi\}$ is presumably related to the two unequal Co-Cl bond distances. This distortion amounts to only $\sim 1\%$ but has a pronounced effect on the orbital energies. One would expect the transferred hyperfine effects to show a similar dependence on internuclear separation. Since the observed anisotropy is quite small, one is led to the conclusion that π interactions between Co^{2+} and Cl^- electrons are nearly as important as σ interactions. This would also account for the relatively large p^δ spin density which is required to explain the small values of $(A_p{}^\xi - A_p{}^\delta)$ and $(A_p{}^\zeta - A_p{}^\delta)$.

B. Antiferromagnetic-State Analysis

In principle, the 0°K chlorine hyperfine fields in $CoCl_2 \cdot 2H_2O$ can be calculated from the hyperfine constants obtained from the paramagnetic state experiments. This assumes that all of the spin unpairing in the chlorine orbitals results from interactions with the two nearest Co^{2+} ions, since these ions have a parallel spin configuration in both paramagnetic and antiferromagnetic states. For this reason the low-temperature measurements do not lead to a separation of the two Co—Cl bond contributions to the net hyperfine field. In the absence of any magnetic fields or exchange interactions the 0°K hyperfine fields are given by

$$H_{\rm hf}{}^r = -(\gamma_N \hbar) A^{rr} \bar{S}^r, \tag{5.12}$$

where $\bar{S}^r$ is the 0°K expectation value of S^r and is related to the fictitious spin $\sigma = \frac{1}{2}$ by the appropriate g_S value.

$$\bar{S}^r = \tfrac{1}{2} \sigma g_S{}^r. \tag{5.13}$$

Combining the calculated ground-state $g_S{}^r$ values (Table V) with (5.9), (5.12), and (5.13) yields

$$\begin{aligned} H_{\rm hf}{}^\xi &= 20 \pm 1 \text{ kOe}, \\ H_{\rm hf}{}^\zeta &= 34.3 \pm 0.8 \text{ kOe}, \\ H_{\rm hf}{}^\delta &= 36.4 \pm 0.5 \text{ kOe}. \end{aligned} \tag{5.14}$$

The effect of exchange interactions on the magnetic moment could be neglected in the paramagnetic state because of mutual cancellation of ferromagnetic and antiferromagnetic contributions. In the ordered state, however, this neglect is not justified. We treat the exchange in terms of an effective exchange field

$$H_E{}^r = 2(g^r\mu_B)^{-1}\sigma(J_0z_0 - J_1z_1 + J_2z_2), \quad (5.15)$$

where $g^r = g_L{}^r + g_S{}^r$. This field can be estimated for the sublattice magnetization direction. We take $g^\delta = 6.77$ according to Table V and utilize the exchange constants listed in Sec. II. The result is

$$H_E{}^\delta = 76.9 \text{ kOe}. \quad (5.16)$$

The exchange energies are smaller than the separation between the two lowest single-ion doublets. Therefore it is possible to estimate the enhancement of $|\bar{S}^r|$ by including a second-order correction according to (4.17).

$$\Delta\bar{S}^\delta = H_E{}^\delta b_S{}^\delta = -0.059. \quad (5.17)$$

Thus $|\bar{S}^\delta|$ is increased by approximately 5% to give $\bar{S}^\delta$ (total) $= -1.30$. This increase is sufficiently small that other internal field contributions to $\bar{S}^\delta$, such as dipole fields, need not be considered. The predicted 0°K hyperfine field therefore becomes

$$H_{\rm hf}{}^\delta(\text{calculated}) = 38.2 \pm 0.8 \text{ kOe}. \quad (5.18)$$

The observed internal field is 27.6 kOe. To obtain the magnetic hyperfine contribution to this field, it is necessary to calculate the 0°K dipole field at a chlorine position. For the two-sublattice spin configuration obtained in I the appropriate lattice sum (5.2) gives

$$\mathfrak{D}^{\delta\delta} = -0.1872 \times 10^{24} \text{ cm}^{-3}. \quad (5.19)$$

The single-ion moment is

$$\bar{\mu}^\delta = g^\delta\sigma\mu_B = 3.38\mu_B. \quad (5.20)$$

The exchange enhancement of $\bar{\mu}^\delta$ can be estimated from

$$\Delta\bar{\mu}^\delta = H_E{}^\delta(\tfrac{3}{2}kb_L{}^\delta - 2b_S{}^\delta)\mu_B = 0.17\mu_B. \quad (5.21)$$

The total 0°K moment is therefore estimated to be $3.55\mu_B$. This agrees reasonably well with the measured value[2] of $3.2 \pm 0.2\mu_B$ in the high-field ferromagnetic state. Using the calculated moment (for reasons of self-consistency) the dipole field becomes $H_d{}^\delta = -6.2$ kOe and consequently

$$H_{\rm hf}{}^\delta(\text{observed}) = 33.8 \text{ kOe}. \quad (5.22)$$

The difference between the calculated (5.18) and observed (5.22) 0°K hyperfine fields is greater than the maximum estimated uncertainty in our analysis. It is tempting to attribute the reduction in $H_{\rm hf}{}^\delta$ to zero-point spin deviations. The resulting reduction in $\bar{S}^\delta$ is probably of the order of a few percent. Another possible reduction mechanism involves interchain transferred hyperfine interactions. The antiferromagnetic interchain exchange interaction has been postulated[1] to arise from Co-Cl-Cl-Co super-exchange paths. The chlorine ions in these bridges lie along [010] (Fig. 1) and probably have strongly overlapping s and p orbitals. Furthermore, the induced moments of the chlorine ions in each pair are oppositely directed along [010]. Thus, if transferred hyperfine effects between the chlorine ions are important, it is likely that they would reduce the effective spin density on each ion in the ordered state. From the difference between the observed hyperfine field in the antiferromagnetic state and that calculated from the paramagnetic state data it should be possible to determine the magnitude of this effect. Unfortunately, the estimated accuracy of our calculation is insufficient to permit a quantitative determination, particularly since the measured moment appears to be somewhat smaller than the calculated one. Qualitatively, however, it appears from our data that Cl—Cl interactions may account for as much as 5% of the measured hyperfine interactions.

VI. ELECTRIC FIELD GRADIENT AT CHLORINE NUCLEUS

We now return to an examination of the chlorine electric field gradient (EFG) in $CoCl_2 \cdot 2H_2O$. The EFG may be partitioned into two parts

$$eq = eq_{\rm lattice} + eq_{\rm atom}. \quad (6.1)$$

The first term represents contributions from charge distributions associated with all atoms in the crystal exterior to the atom at which the EFG is evaluated. The second term represents the contribution from any nonspherical electronic charge distribution of the central atom itself. This separation is very similar to that employed in the magnetic case. In contrast to the latter, however, the lattice EFG term is not small in $CoCl_2 \cdot 2H_2O$ compared to the more interesting central-atom term. A determination of the latter would provide important information about the configuration of the chlorine valence electrons. Thus, nuclear-quadrupole-interaction studies in free molecules and molecular crystals where $eq_{\rm lattice}$ is either absent or small have added considerably to the understanding of the nature of the chemical bond. In crystals with appreciable ionic character, however, the lattice contribution may dominate. Unfortunately, in ionic crystals it is not possible, in general, to calculate $eq_{\rm lattice}$ with sufficient accuracy to yield $eq_{\rm atom}$ from experiment.

Despite the difficulties discussed above it was deemed useful to estimate $eq_{\rm lattice}$ for the chlorine site in $CoCl_2 \cdot 2H_2O$. This view was motivated by recent attempts to improve the reliability of lattice EFG calculations.[23,24] Furthermore, the crystal twinning problems which were encountered in our studies on $CoCl_2 \cdot 2H_2O$ made it desirable to verify the orientation of the EFG X axis

[23] D. V. G. L. Narasimha Rao and A. Narasimhamurty, Phys. Rev. 132, 961 (1963).
[24] R. R. Sharma and T. P. Das, J. Chem. Phys. 41, 3581 (1964).

on the basis of a calculation. For example, if the orientation of the a axis relative to a^* had been assigned incorrectly in our single crystal specimens, the signs of λ_X, λ_ξ, and λ_α would have to be reversed. In that case the X, ζ, and α directions would have to be associated with the short rather than long Co—Cl bond.

The simplest model of the lattice EFG replaces the actual charge distribution by point charges situated at the lattice positions.

$$\{\nabla \mathcal{E}\}_{\text{lattice}} = (1-\gamma_\infty) \sum_i e_i \{\mathfrak{D}_i\}, \qquad (6.2)$$

where γ_∞ is the Sternheimer antishielding constant[25] which corrects for the distortion of the central-ion charge distribution which is caused by the combined action of the external and nuclear potentials. It is this factor which probably introduces the greatest uncertainty into eq_{lattice}, at least in the case of heavy negative ions such as Cl^-. The sum in (6.2) is taken over all nonequivalent sites in the crystal. The point charge at each of these sites is taken as e_i. The individual lattice sums are defined by (5.2). The same computer code was used as in the magnetic dipole-field calculations. The lattice sums were again restricted to points within a spherical volume of radius 200 Å centered at the chlorine position. Room-temperature x-ray lattice constants were used except for the hydrogen positions for which the estimates given in I were used. The cobalt and chlorine charges (in units of $|e|$) were taken as $+2$ and -1, respectively. The appropriate oxygen and hydrogen charges were estimated to be -1.06 and $+0.53$, respectively, on the basis of the static dipole moment of the water molecule ($\mu = 1.85 \times 10^{-18}$ esu). The results are summarized in Table VI. The listed values give

$$\begin{aligned} \nu_Q{}^{35} &= 0.175(1-\gamma_\infty) \text{ Mc/sec}, \\ \eta &= 0.31, \\ \lambda_X &= -10.8°. \end{aligned} \qquad (6.3)$$

The major principal axis coincides with b in agreement with experiment. If we take $\gamma_\infty = -27$ according to an estimate by Burns and Wikner[26] we obtain $\nu_Q = 4.9$ Mc/sec compared to the experimental room-temperature value 5.066 Mc/sec. It is reassuring that the calculated shift of the X principal axis relative to a^* is in the observed direction. However, the calculated $|\lambda_X|$ is significantly smaller than the observed value. This suggests that electrons in the Co—Cl bonds may contribute appreciably to the chlorine-site EFG. This would shift the EFG principal axes closer toward the bond directions than predicted by the point-charge model.

TABLE VI. Results of point-charge calculations of $\{\nabla \mathcal{E}\}_{\text{lattice}}$ for the chlorine site in $CoCl_2 \cdot 2H_2O$ [in units of $(1-\gamma_\infty)e \times 10^{24}$ cm^{-3}] based on the charge assignment given in the text. The coordinate system is $x = a^*$, $y = c$, $z = b$. Elements not listed are zero by symmetry.

Position	V^{xx}	V^{yy}	V^{zz}	V^{xy}
Co	−0.1006	−0.1331	0.2337	−0.0079
Cl	0.0170	0.0252	−0.0422	−0.0027
O	−0.0270	−0.0382	0.0652	0.0118
H	0.0665	0.0661	−0.1326	−0.0082
total	−0.0441	−0.0800	0.1241	−0.0070

[25] R. Sternheimer, Phys. Rev. **80**, 102 (1950).
[26] G. Burns and E. K. Wikner, Phys. Rev. **121**, 155 (1961).

The close agreement between calculated and observed values of ν_Q must not be taken too seriously because of the uncertainty connected with the value of $(1-\gamma_\infty)$. Estimates[26] of this constant for ^{35}Cl have covered the range ~10–60. Thus not much confidence can be attached to any estimate of the absolute magnitude of eq_{lattice}. On the other hand, orientations of principal axes, as well as relative values of ν_Q for different crystals are apparently predicted quite reliably by the point-charge model.

Attempts to improve the point-charge model by incorporation of induced dipole effects have had little success. Although the induced dipole contributions to the computed EFG are quite large, the agreement with experiment is usually poorer than for the point-charge model. For example, recent calculations[27] of the point-charge EFG at the chlorine site in $CuCl_2 \cdot 2H_2O$ reproduced the measured values reasonably well; inclusion of induced dipole contributions,[23] however, resulted in marked disagreement with experiment.[27] It appears, therefore, that the point-charge model is capable of qualitative predictions of the EFG in ionic crystals. A significant improvement of this model, however, is not yet available.

VII. SUMMARY AND DISCUSSION

This paper has been concerned with the elucidation of three tensor properties of $CoCl_2 \cdot 2H_2O$. These are the bulk paramagnetic susceptibility, the chlorine quadrupole interaction, and the chlorine magnetic-hyperfine interaction. Principal values and principal-axis orientations were determined in all three cases with reasonable accuracy.

The paramagnetic susceptibility of $CoCl_2 \cdot 2H_2O$ in the range 20–120°K is characterized by extreme rhombic anisotropy. The principal axis orientations of the susceptibility tensor are related to the bond directions associated with the two oxygen and four chlorine ions surrounding each cobalt ion. The major axis coincides with the Co—O direction. The smallest principal susceptibility occurs along the short Co—Cl direction, while the intermediate principal susceptibility occurs along the long Co—Cl bond. The anisotropy of the ac plane susceptibility is evidently caused by the unequal Co—Cl bond lengths. The large magnitude of anisotropy is somewhat surprising, however, in view of the small difference (~1%) between the two separations.

[27] W. J. O'Sullivan, W. W. Simmons, and W. A. Robinson (to be published).

We have been able to account for the observed susceptibilities on the basis of a simple parametric model of the crystal field. The choice of model was dictated by the desire to keep the number of adjustable parameters in the calculation at a minimum. Satisfactory agreement between theory and experiment was obtained with a two-parameter rhombic perturbation of the orbital energies within $^4T_1(^4F)$ in the presence of spin-orbit coupling. The best fit of theory to experiment is obtained with an asymmetry parameter $\kappa=0.0$. This value represents the largest deviation from axial symmetry obtainable with the present model. The noncubic crystal-field perturbations were found to be significantly larger than the spin-orbit interaction. As a consequence, the six Kramers doublets arising from $^4T_1(^4F)$ are predicted to fall into three approximately equally spaced pairs. The calculated doublet separation of the lowest pair in the paramagnetic state is 136 cm^{-1}. This separation is small enough that thermal excitations from the ground state modify the observed susceptibilities significantly.

The paramagnetic-state calculations of the susceptibility ignored exchange effects. This neglect is justified by the vanishingly small Weiss constant reported in I. The agreement between observed and calculated susceptibilities found in the present work also supports the view that the ferromagnetic and antiferromagnetic exchange energies of $CoCl_2\cdot 2H_2O$ are essentially of equal magnitude.

The chlorine nuclear-quadrupole-interaction parameters have been determined from measurements in the paramagnetic state. The analysis was complicated by the presence of large magnetic-hyperfine effects. The EFG parameters determined from experiment are in reasonable agreement with predictions of the point-charge model. In particular, the principal axis orientations of the EFG are predicted rather accurately. The calculated principal values on the other hand are quite uncertain because (1) the correct value of the antishielding factor is not known, and (2) the contribution to the EFG from the chlorine valence electrons has not been considered. This latter contribution appears to be significant since the observed orientations of the EFG principal axes in the *ac* plane lie appreciably closer to the Co—Cl bond directions than predicted by the point charge model.

The chlorine magnetic field-shift parameters have been deduced in the range 55–90°K. The field shifts were shown to be describable by a symmetric second-rank tensor form. By combining the measured field shifts with calculated thermal expectation values of the spin it was possible to obtain the magnetic-hyperfine coupling constants for the chlorine nucleus in $CoCl_2\cdot 2H_2O$. The transferred hyperfine fields were shown to be much larger than the dipolar fields. In contrast to the magnetic susceptibility, the magnetic-hyperfine tensor is nearly isotropic. This result is somewhat unexpected since the transferred hyperfine effects associated with the two Co—Cl bonds should be quite different. This follows from the strong dependence of $\{\mathbf{A}\}$ on bond distance which has been demonstrated in previous studies.[11] Thus we are forced to conclude that both σ and π interactions with chlorine p electrons contribute significantly to the total transferred hyperfine interaction. In this way the contribution from each of the bonds becomes nearly isotropic. The sign of the measured anisotropy shows that the spin density in chlorine p^ξ and p_ξ orbitals is somewhat larger than in the p^δ orbital. The accuracy of these results is dependent, of course, on the validity of the assumption that transferred orbital effects are unimportant in $CoCl_2\cdot 2H_2O$.

The 0°K chlorine internal field of 27.6 kOe in $CoCl_2\cdot 2H_2O$ compares with recently measured internal fields of 7.5 kOe in $CoCl_2\cdot 6H_2O$,[28] and 77 kOe in $FeCl_2$.[29] A more detailed comparison with our results, (5.11), is afforded by a recent study of the chlorine NMR in $CuCl_2\cdot 2H_2O$ in which a separation of isotropic and anisotropic contributions to $\{\mathbf{A}\}$ was accomplished.[27] The measured values in $CuCl_2\cdot 2H_2O$ are (using our notation) $A_s=8.2\times10^{-4}$ cm^{-1}, $A_p{}^\xi-A_p{}^\zeta=5.6\times10^{-4}$ cm^{-1}, and $A_p{}^\zeta-A_p{}^\delta=0.0$, where ξ is the direction of the short Cu—Cl bond. The difference between the two Cu—Cl bond lengths is about 30% and the measured hyperfine interaction is found to be completely dominated by the short bond. The σ interactions in $CuCl_2\cdot 2H_2O$ are seen to be much larger than the π interactions, in contrast to the situation in $CoCl_2\cdot 2H_2O$.

ACKNOWLEDGMENTS

The author is greatly indebted to D. W. Alderman for performing the initial chlorine Zeeman-splitting experiments, and to Dr. W. J. O'Sullivan and Dr. B. Morosin for many helpful discussions. It is also a pleasure to acknowledge the valuable technical assistance of D. C. Barham throughout the course of this work.

[28] R. T. Schumacher and R. L. Hartman, Bull. Am. Phys. Soc. **10**, 316 (1965).

[29] S. Segel and W. H. Jones, Bull. Am. Phys. Soc. **9**, 620 (1964).